Thermal properties of semiconducting InAs nanowires

Antti Jokiluoma

School of Science

Thesis submitted for examination for the degree of Master of Science in Technology.

Espoo 30.5.2017

Thesis supervisor:

Prof. Jukka Pekola

Thesis advisor:

Dr. Ville Maisi

Aalto University
School of Science

AALTO UNIVERSITY
SCHOOL OF SCIENCE

ABSTRACT OF THE
MASTER'S THESIS

Author: Antti Jokiluoma

Title: Thermal properties of semiconducting InAs nanowires

Date: 30.5.2017 Language: English Number of pages: 5+45

Department of Applied Physics

Professorship: Physics of Advanced Materials

Supervisor: Prof. Jukka Pekola

Advisor: Dr. Ville Maisi

Semiconducting nanowires have been studied intensively during the past few decades and are nowadays used in many applications, for example in small electronic circuits. They are usually tens of nanometers in diameter and several micrometers in length, and can be fabricated with a good control of size and composition and with high-quality crystal structure.

One potential application for semiconducting nanowires is calorimetric single-photon detector, a nanoelectronic device used to detect single quanta of energy in the microwave regime. This device operates by sensing small temperature changes on a nano-sized metal island that heats up when it absorbs single photons. Currently, the absorber island is a thin film of copper or silver, but the device could possibly be enhanced by using InAs nanowires instead.

In this thesis, the thermal properties of semiconducting InAs nanowires are studied in order to determine the strength of the electron-phonon coupling in a nanowire. Devices both with tunnel junctions and ohmic contacts to the nanowire were fabricated and their current-voltage characteristics were measured at low temperatures. The setup with two subsequent superconductor-insulator-nanowire tunnel junctions was found to be unsuitable for this purpose because of the undesired proximity effect in the nanowire due to the superconducting aluminum connected to the nanowire. Another approach was to measure the temperature-dependent supercurrent flowing between two Al electrodes contacted directly to the nanowire with ohmic contacts. Preliminary results obtained from the supercurrent measurement are discussed in this thesis but determining the electron-phonon coupling constant requires further studies.

Keywords: nanowire, indium arsenide, electron-phonon coupling, superconducting junction

AALTO-YLIOPISTO
PERUSTIETEIDEN KORKEAKOULU

DIPLOMITYÖN
TIIVISTELMÄ

Tekijä: Antti Jokiluoma

Työn nimi: Puolijohtavien InAs-nanolankojen lämpöominaisuudet

Päivämäärä: 30.5.2017 Kieli: Englanti Sivumäärä: 5+45

Teknillisen fysiikan laitos

Professuuri: Kehittyneiden materiaalien fysiikka

Työn valvoja: Prof. Jukka Pekola

Työn ohjaaja: TkT Ville Maisi

Puolijohdenanolankoja on tutkittu intensiivisesti viimeisten vuosikymmenten aikana, ja niitä käytetään nykyään useissa sovelluksissa muun muassa pienikokoisissa sähköpiireissä. Ne ovat halkaisijaltaan tyypillisesti kymmeniä nanometrejä ja pituudeltaan useita mikrometrejä. Nanolankojen valmistusprosessissa pystytään kontrolloimaan tarkasti niiden kokoa ja koostumusta ja saamaan aikaan hyvälaatuinen kiderakenne.

Eräs mahdollinen sovelluskohde puolijohtaville nanolangoille on kalorimetrinen yksifotonidetektori, joka on yksittäisten mikroaaltojen taajuusalueella olevien energiakvanttien havaitsemiseen käytettävä nanoelektroninen laite. Laitteen toimintaperiaate perustuu pienten lämpötilamuutosten havaitsemiseen nanokokoisella metallisaarekkeella, joka lämpenee fotonin absorboituessa siihen. Tällä hetkellä absorberina käytetään ohuita kupari- tai hopeakalvoja, mutta laitteen toimivuutta voitaisiin mahdollisesti parantaa käyttämällä InAs-nanolankoja metallikalvojen sijaan.

Tässä työssä tutkittiin puolijohtavien InAs-nanolankojen lämpöominaisuuksia niiden elektroni-fononikytkennän määrittämiseksi. Tätä varten valmistettiin rakenteita, joissa nanolangan ja mittausjohtimien välillä oli joko tunneliliitos tai ohminen liitos. Näiden rakenteiden virta–jännite-käyrä mitattiin matalissa lämpötiloissa. Rakenne, jossa oli kaksi peräkkäistä suprajohde-eriste-nanolanka-liitosta, ei toiminut halutulla tavalla, koska alumiini indusoi ei-halutun suprajohtavuuden nanolankaan. Toinen lähestymistapa oli mitata lämpötilasta riippuvaa supravirtaa kahden ohmisella kontaktilla nanolankaan liitetyn johtiminen välillä. Tässä työssä tarkastellaan supravirtamittausten alustavia tuloksia, mutta elektroni-fononikytkennän määrittämiseksi tarvitaan lisää tutkimusta.

Avainsanat: nanolanka, indiumarsenidi, elektroni–fononi-kytkentä, suprajohtava liitos

Acknowledgements

This work was carried out in the PICO group of the Low Temperature Laboratory at Aalto University. I started working there as a summer student in 2015 and stayed for the rest of my studies first part-time and then doing this master's thesis. This time has given me valuable experience in the research work and the academic world.

I want to thank professor Jukka Pekola for giving me the opportunity to work in his group and showing me how great results are achieved by passionate and hard work. I am greatly indebted to my instructor Dr. Ville Maisi for valuable advice and support during my work. I would also like to express special thanks to other colleagues in the group, who have taught me many things especially related to low temperature measurements, helped me always with my problems and been great company not only in the laboratory but also in free time. You have made my time in the group enjoyable.

I am grateful to my family for all the support during my studies and to my friends for sharing many great moments with me along the way. Finally, I would like to thank Erika for her continuous encouragement and understanding.

Helsinki, 30.5.2017

Antti Jokiluoma

Contents

Chapter 1

Introduction

For many decades, a strong trend in electronics industry has been the development of even smaller and smaller components. That has made it possible to increase memory and computation power of digital circuits and reduce the costs of production. The miniaturization has also led to new innovations in this field. This development has followed rather precisely the Moore's Law, which states that every eighteen months, the size of transistors on microprocessor chips reduces to half, thus doubling the computation power [1]. Lately, the size of the components has started to reach the physical limits – it is close to the size of single atoms or molecules [2]. This has increased the interest to study new physics and create new technologies to keep the development going on.

Nanotechnology covers a wide range of technologies that have a common property related to the size of a system: at least one dimension is less than 100 nanometers in length. One specific branch of nanotechnology is nanoelectronics which deals with nanoscale electronic devices. These structures are so small, that often quantum mechanics starts to play role in the behaviour of the systems. For example, single-electron transistors are working with the accuracy of single electrons [3] and would provide much lower power consumption and higher operating speed than conventional transistors. One future goal of nanoelectronics is the realization of a quantum computer, in which the computation is based on quantum bits, or qubits, that use quantum mechanical principles in their operation [4].

The rich properties of semiconductors and superconductors play often a significant role in nanoelectronic devices [5, 6]. The conductivity in semiconductors is typically smaller than in metals. They are useful materials in many electronic systems because their conductivity can be controlled by doping or applying an electric potential. They can be insulating under certain conditions and made conductive by changing their electric potential. This basic property can be explained with the band structure of

the electrons in a semiconductor. The band gap dividing the conduction and valence bands is either smaller than in insulators, so that the thermal energy is large enough to excite some of the electrons to the conduction band, or doping brings the Fermi level sufficiently close to one of the band edges.

Another important class of materials is superconductors, which are widely used in nanoelectronic devices, especially because of the diverse properties of the junctions involving superconductors. There are several macroscopic phenomena characteristic to superconductors. First, the resistance vanishes below a certain critical temperature T_C, allowing a dissipationless supercurrent to flow in a superconductor, without any Joule heating arising from the resistivity. Superconductors exhibit also perfect diamagnetism when the external magnetic field is weak enough. A third property, and the most important for the behaviour of the superconducting junctions, is the gap in the energy spectrum for single-particle excitations. [6]

Nanoelectronics devices made of metals, superconductors, semiconductors, insulators, or the combination of these, can be used to study new physical phenomena in many different fields. One particular area is quantum thermodynamics, that has attracted a lot of interest [7]. A useful tool for new experiments would be a single-photon detector, a device that would allow the detection of a single quantum of electromagnetic field. An ultrafast single-photon detector for microwave frequencies has been under development in PICO group at Aalto University [8]. It is based on calorimetric detection of energy by measuring the temperature change of a small metal island due to an absorption of energy. This kind of fast thermometer can be used to measure the thermal relaxation of a metal island. Currently, the energy resolution of the device corresponds to a 2 K energy quantum. To enhance this further, new alternatives for the absorber material have been proposed. The motivation of the work in this thesis was to study the feasibility of semiconducting InAs nanowires for the calorimetric single-photon detector. There are several interesting properties that could be useful in this application, such as the possibility to tune the properties of the island by a gate voltage, a smaller electron density and possibly smaller coupling between the electrons and phonons, leading to a longer relaxation time for the temperature on the island.

Semiconducting nanowires are thin and long objects that are usually some micrometers in length and have a diameter of tens or hundreds of nanometers. The research activity on semiconducting nanowires has increased significantly during the past two decades, and various different applications for them have been developed or proposed. Many differences between the nanowires and their bulk correspondents result from the one-dimensionality, which affects the physical properties of the material. For

example, silicon in bulk is both a good thermal and electrical conductor, but Si nanowires are however thermal insulators while staying as electrical conductors. [9]

The applications utilizing nanowires cover a wide range of different fields. In electronics, nanowires are used for example as a building block of field-effect transistors [10, 11]. The benefits compared to the conventional electronics is low voltage operation and high gate sensitivity, and they could be used in low-power electronics. Semiconducting nanowires can be used also in photonics [12], for example as nano-sized lasers or photon detectors in photonic circuits and miniaturized sensors. Another potential field is energy conversion, in which nanowires could be used in photovoltaic, thermoelectric and chemical energy storage applications [13]. Because of their small size, nanowires provide also possibilities in biological applications, where they can be brought in interaction with living cells [9]. An interesting discovery is also the realization of Majorana modes in semiconducting nanowires proximized with superconductor [14], which could offer a platform for topilogical quantum computation [15].

One factor driving the field of semiconductor nanowires is the progress in the fabrication methods [13]. Nanowires can be produced by various methods that can be divided into two categories: top-down and bottom-up [9]. In top-down methods, the starting point is a bigger piece of material, which is then shaped for example by etching and nanoimprinting. Bottom-up method starts with a catalyst particle, for example a gold atom, and then the wire is grown from individual atoms, resulting in a well-ordered structure. Both methods have their advantages and limitations, depending on the application. The InAs nanowires used in this thesis were grown by bottom-up methods.

This thesis is structured as follows. Chapter 2 gives a description of different superconducting junctions and the thermometry based on them. The operation principle of a calorimetric single-photon detector and the properties and growth of semiconducting InAs nanowires are introduced. In Chapter 3, the cryogenic methods used in this thesis are briefly explained, followed by the description of the sample fabrication methods and the measurement setup. The results of the experiments are presented in Chapter 4, and finally a conclusion is given in Chapter 5.

Chapter 2

Theoretical background

This chapter introduces the physical phenomena that are important for understanding the measurements conducted in this thesis with the InAs nanowires. First, I describe the physics behind different superconducting junctions and their use as thermometers. Then the operation principle of a calorimetric single-photon detector is explained, and a short overview of the basic properties of semiconducting nanowires is presented, along with the description of the growth process of InAs nanowires. Finally, the electron-phonon coupling of InAs nanowires and previous work on it is addressed.

2.1 Superconducting junctions

The phenomena taking place in superconductors can be understood with a microscopic theory which is called as the BCS theory [6]. Electric current is carried by Cooper pairs formed by two coupled electrons. Cooper pairs, unlike single electrons, behave as bosons and can condense into the same quantum ground state. In order to create a single-particle excitation (quasiparticle) in a superconductor, a Cooper pair needs to be broken. This requires energy and results to an energy gap

$$\Delta_{T=0} = 1.764 k_B T_C, \tag{2.1}$$

where k_B is the Boltzmann constant and T_C the critical temperature of the superconductor. When the temperature T approaches T_C, the gap vanishes.

To understand the operation of the devices measured in this thesis, three different superconducting junctions have to be considered. Two of them are tunnel junctions, either between normal metal and superconductor (NIS junction) or between two separate superconductors (SIS junction). The third case is a weak superconducting link between two superconductors (SNS junction).

2.1.1 Tunnel junctions

A NIS junction consists of normal metal and superconducting electrodes separated by an insulating barrier. The tunneling rates for electrons across a barrier can be calculated with the Fermi golden rule, resulting in the rates

$$\Gamma_{L\to R} = \frac{1}{e^2 R_T}\int_{-\infty}^{\infty} dE n_L(E) n_R(E + eV_{bias}) f_L(E)[1 - f_R(E + eV_{bias})] \tag{2.2}$$

and

$$\Gamma_{R\to L} = \frac{1}{e^2 R_T}\int_{-\infty}^{\infty} dE n_R(E - eV_{bias}) n_L(E) f_R(E - eV_{bias})[1 - f_L(E)], \tag{2.3}$$

where R_T is the asymptotic resistance of the tunnel junction at large voltages, V_{bias} the voltage difference between the two electrodes, $n_{L/R}(E)$ the density of states (DOS) and $f_{L/R}$ the Fermi function in the left or right electrode, giving the energy distribution of the electrons in the normal metal and the quasiparticles in the superconductor. The Fermi function can be written as

$$f_{N,S}(E) = \frac{1}{(1 + e^{E/(k_B T_{N/S})})}, \tag{2.4}$$

where $T_{N/S}$ is the electron temperature of the normal metal or superconductor and E is the energy of an electron or a quasiparticle with respect to the Fermi level [16]. The electric current can be calculated from the rates as

$$I(V_{bias}) = e[\Gamma_{L\to R}(eV_{bias}) - \Gamma_{R\to L}(-eV_{bias})]. \tag{2.5}$$

The density of states (DOS) in the superconductor is described by the BCS DOS as

$$n_S(E) = \frac{|E|}{\sqrt{E^2 - |\Delta|^2}}\Theta(|E| - |\Delta|), \tag{2.6}$$

where Θ is the Heaviside step function. In normal metal, the DOS is constant. The product of the Fermi function and the DOS is illustrated for NIS and SIS junctions in Fig. 2.1.

At low enough temperatures, when $T_{N/S} << \Delta/k_B$, the electrons do not have enough energy to populate quasiparticle states in the superconductor. However, when a bias voltage is applied across the junction, the Fermi level in the normal metal is shifted with respect to the superconductor, and the electrons can tunnel

into the free states above the energy gap, as illustrated in Fig. 2.1a.

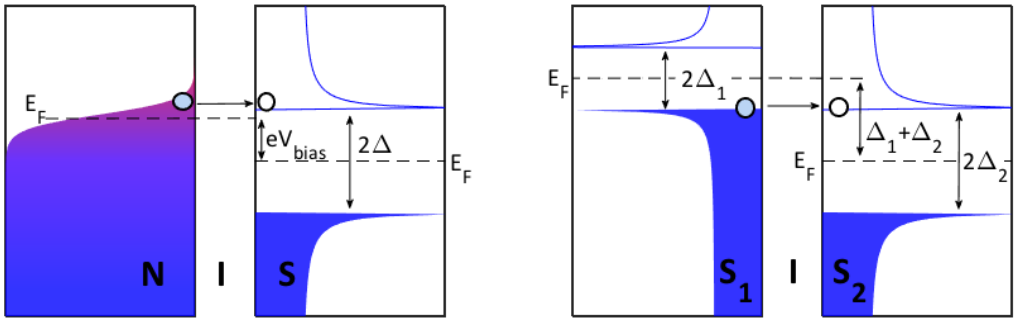

(a) (b)

Figure 2.1: a) Schematic illustration of the Fermi function in a normal metal and the BCS density of states in a superconductor. The electrons can tunnel from the normal metal into the free states above the energy gap in the superconductor. The Fermi levels are shifted with respect to each others by applying a bias voltage. b) The BCS DOSs of two different superconductors, with the energy gaps Δ_1 and Δ_2. When the applied bias voltage is $|eV_{bias}| \geq \Delta_1 + \Delta_2$, the electrons can tunnel between superconductors S_1 and S_2.

For metals, $n_N(E) = 1$, and the tunneling rates from superconductor to normal metal and vice versa become

$$\Gamma_{S\to N} = \frac{1}{e^2 R_T} \int_{-\infty}^{\infty} dE n_S(E) f_S(E)[1 - f_N(E + eV_{bias})] \tag{2.7}$$

and

$$\Gamma_{N\to S} = \frac{1}{e^2 R_T} \int_{-\infty}^{\infty} dE n_S(E) f_N(E - eV_{bias})[1 - f_S(E)]. \tag{2.8}$$

The electric current for the NIS junction according to Eq. (2.5) is

$$I_{NIS} = \frac{1}{2eR_T} \int_{-\infty}^{\infty} dE n_S(E)[f_N(E - eV_{bias}) - f_N(E + eV_{bias})]. \tag{2.9}$$

The current-voltage characteristics for a typical NIS junction is plotted in Fig. 2.2. The shape of the I-V curve is sensitive only to T_N, not to T_S. The thermal excitations in the superconductor result in current flow in two directions, which cancel each other out.

The tunneling between two superconductors is a bit more complex than in the case of a NIS junction, since now the DOSs on both sides of the insulating barrier are described by the BCS DOS (with the energy gap Δ_1 on the left and Δ_2 on the right), as illustrated in Fig. 2.1b. Thus, the tunneling requires a bias voltage corresponding

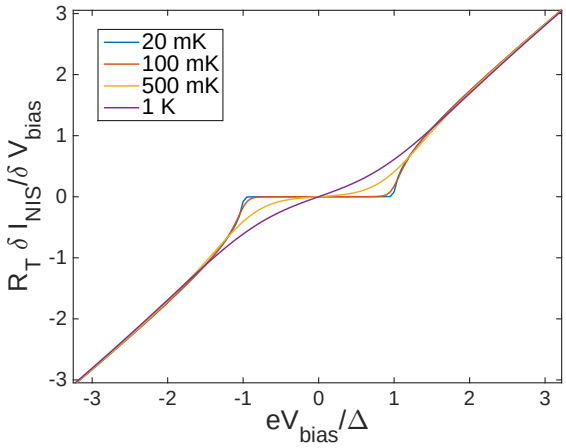

Figure 2.2: The current-voltage characteristics at different temperatures across a typical NIS junction with Al as a superconductor ($T_C = 1.2$ K).

to the energy $\Delta_1 + \Delta_2$, which shifts the Fermi levels such that quasiparticles below the gap on the one side can tunnel to the free states above the gap on the other side. In addition, there is an increase of the tunneling current around the bias $\Delta_1 - \Delta_2$, which shifts the Fermi levels such that thermally activated electrons on one superconductor can tunnel to the free levels on the other side. The I-V characteristics of a SIS junction can be used as a thermometer for the superconductor temperature. The tunneling rate for a SIS junction according to Eq. (2.3) is

$$\Gamma_{S_1 \to S_2} = \frac{1}{e^2 R_T} \int_{-\infty}^{\infty} dE n_{S_1}(E) n_{S_2}(E + eV) f_{S_1}(E)[1 - f_{S_2}(E + eV)]. \tag{2.10}$$

2.1.2 Weak superconducting links

Supercurrent is dissipationless current that flows in a superconductor under certain conditions. In 1962, Brian Josephson predicted that a supercurrent flows also in a circuit, where two superconductors are separated by a weak link, such as an insulating barrier or a short segment of normal metal [17]. The magnitude of the supercurrent in an ideal weak link, without any voltage difference between the superconductors, can be written as

$$I_S(\phi) = I_C \sin \phi, \tag{2.11}$$

where ϕ is the phase difference between the two superconducting electrodes and I_C the critical current.

In SNS junctions, the weak link is for example a normal metal or semiconductor,

and the supercurrent flow is based on the superconducting proximity effect. This phenomenon was observed already before Josephson came up with the mathematical description of the Josephson effect [18]. The proximity effect describes a situation, where superconductor and normal metal are brought in contact with high transparency. As a result, the Cooper pairs can penetrate a small length into the normal metal.

The mechanism behind the proximity effect can be explained by Andreev reflection [19], in which an incident electron with energy E ($E_F < E < \Delta$) arrives to the NS boundary from the normal metal side and pairs up with another electron with energy $-E$ to form a Cooper pair on the other side of the boundary. An additional hole with energy $-E$ but opposite velocity and spin to the incident electron is reflected back to the normal metal. This process is illustrated in Fig. 2.3. Supercurrent transport through a SNS junction can be understood as a sequence of two Andreev reflections [20].

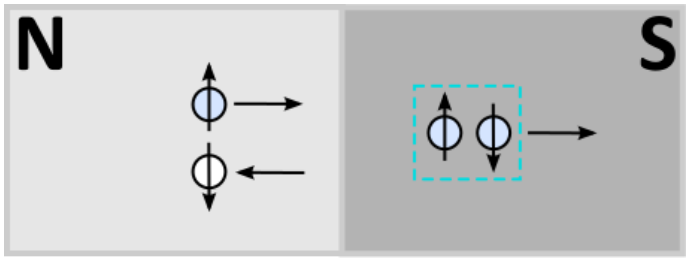

Figure 2.3: Andreev reflection at a NS boundary. The incident electron in the normal metal pairs with another electron, forming a Cooper pair in the superconductor. A hole with opposite velocity is reflected back in the normal metal.

2.1.3 Thermometry based on superconducting junctions

Superconducting junctions can be used as thermometers in mesoscopic scales because their I-V characteristics change with temperature. NIS thermometers are good for detecting the temperature of normal metal islands because the current-voltage characteristics of the junction depends only on the electron temperature of the N electrode, as long as Δ is considered to be independent of the temperature. This becomes evident by considering Eq. (2.8). The temperature dependence of the transport across a NIS junction can be seen in Fig. 2.2.

In SIS junctions, both the supercurrent and the quasiparticle current can be used as a thermometer [21]. The supercurrent depends on the temperature both explicitly and through the temperature dependence in the energy gap. The explicit dependence is hyperbolic and increases as T approaches T_C, unlike the energy gap. However, at low temperatures this dependence is exponentially weak. Also the quasiparticle

current can be expressed again with Eq. (2.3) and utilized for determining the temperature.

Proximity effect thermometers, or SNS thermometers, can be utilized with similar ways as SIS thermometers, i.e., either by measuring the supercurrent or quasiparticle current. One advantage of the SNS thermometers is that the magnitude of the critical current can be made much larger than for the tunnel junctions, since the resistance of the SNS junctions are typically much smaller. The magnitude of the critical current can be easily tuned by changing the junction length for different temperature ranges [22].

2.2 Single-photon detector

Single-photon detection is utilized in many applications nowadays, including single-molecule spectroscopy, metrology, light detection and ranging (LIDAR), various medical applications and many more [23]. It plays a key role also in quantum-information science, where the quantum state of an object is used for computation or communication. Many photonic systems such as photonic qubits require single-photon sources and detectors for operation. Various methods for single-photon detection have been developed for optical photons, but for less energetic photons in the microwave range, new devices are under development [24, 25]. These would open new paths towards quantum computing and serve as a tool for experiments in the field of quantum thermodynamics.

2.2.1 Calorimetry

Ultra-sensitive calorimeters can be used as single-photon detectors, when their energy resolution is large enough to resolve the energy of a single photon. This kind of calorimeter can be made in principle out of a small metallic island. When the island absorbs a photon, the electronic temperature rises by a small amount and then relaxes exponentially back to the bath temperature, as shown in Fig. 2.4. The small temperature rise is detected for example with a NIS thermometer. The thermal model describing the calorimeter is illustrated in Fig. 2.5. The electron-electron scattering is much faster than for electron-phonon scattering, and thus the electrons thermalize internally fast to a well defined temperature. When the calorimeter absorbs energy, the electron temperature first rises and then relaxes back to the bath temperature following the heat balance equation

$$C_e \dot{T}_e = \dot{Q}_{tot}, \tag{2.12}$$

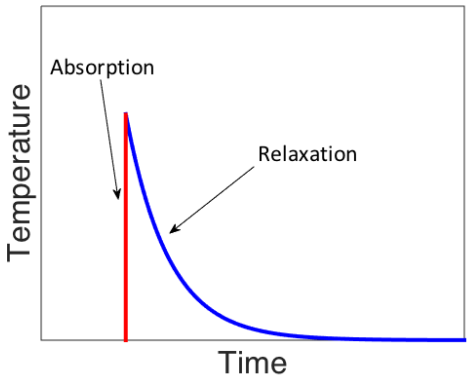

Figure 2.4: The basic operation principle of the single-photon detector. The red line describes the temperature rise of the electrons in the normal metal island after an absorption of an energy quantum. After that, the temperature relaxes back to the bath temperature, which is described with the blue curve.

where C_e is the electronic heat capacity and Q_{tot} the total heat flow between the electrons on the island and the environment. If one considers only the heat flow through the electron-phonon scattering, the rate can be written as

$$\dot{Q}_{e-p} = \Sigma V(T_e^5 - T_p^5), \tag{2.13}$$

where Σ is material dependent electron-phonon coupling constant and V is the volume of the normal metal island [26].

The energy resolution depends on the heat capacity of the island. For many metals, a good approximation can be obtained with the free electron model as

$$C_e = \frac{\delta E}{\delta T} = \gamma V T_e, \tag{2.14}$$

where γ is the Sommerfeld constant. The heat capacity can be made smaller by decreasing the size of the absorber or the operating temperature.

The time constant for the relaxation of T_e back to the bath temperature is given by

$$\tau = \frac{\gamma}{5\Sigma T_e^3}. \tag{2.15}$$

The state-of-the-art in the energy resolution with Ag island corresponds currently to a 2 K energy quantum [27]. Improvements can be done by enhancing the filtering in the setup and thus decreasing the operating temperature, by decreasing the noise by using better first stage amplifier, and by proximizing the normal metal wire and measuring the supercurrent across a SIS junction instead of the quasiparticle current.

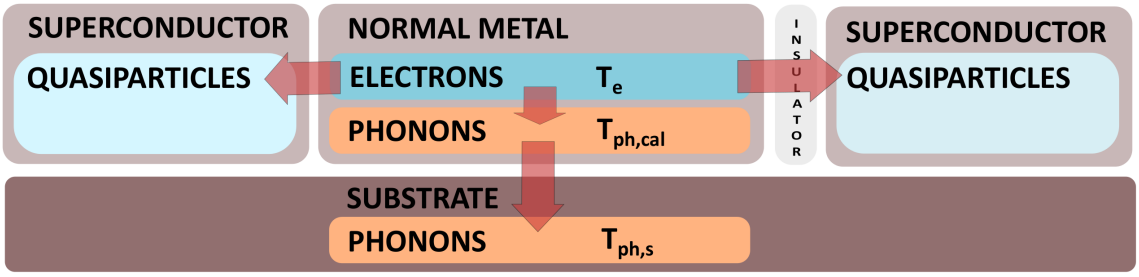

Figure 2.5: Thermal model showing the heat paths (red arrows) from the electrons in the normal metal to the substrate phonons and quasiparticles. The heat flow to the superconductors is much smaller than to phonons, and can be ignored in many cases. The phonons in the metal and substrate are also strongly coupled and can be assumed to have the same temperature in the simpest model.

One possibility is also to choose different absorber material which would be more suitable for the device operation, for example by having a smaller electron-phonon coupling. Semiconducting InAs nanowires could be a suitable canditate for the absorber, and the goal of the project started in this thesis is to investigate this by measuring the heat capacity of the nanowire.

2.2.2 RF thermometer

Ultra-sensitive calorimeters allowing fast measurement of temperature are needed for single-photon detection, which would enable many experiments and applications in the field of mesoscopic physics and quantum thermodynamics. RF-NIS thermometer is good for that purpose, since it can be operated at microwave frequencies to detect the temperature of a normal metal island. In the following, the operating principle of this kind of thermometer is described.

The central part of the thermometer is a normal metal island, that works as an absorber. Instead of directly measuring the quasiparticle current through the NIS junction, the operation is based on measuring the transmission of a readout resonator to which the NIS junction is connected. A schematic of the setup is shown in Fig. 2.6. The readout resonator consists of an on-chip inductor and the parasitic capacitance from the sample to ground. The transmittance of the resonator circuit depends on the conductance of the NIS junction, and thus can be used as a measure of temperature of the normal metal island. The island is thermally well isolated from the environment because it is connected only to the superconducting electrodes, which are poor thermal conductors.

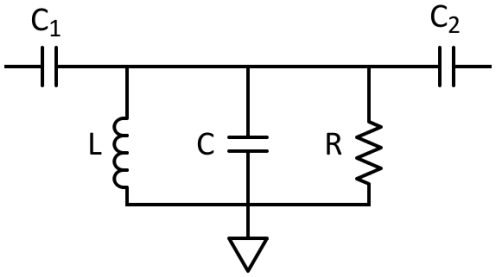

Figure 2.6: A schematic showing the setup, in which the RF-NIS thermometer is operated. RF signal is applied through the capacitor C_1, and the transmitted power is measured after C_2. L is the on-chip inductor and C the parasitic capacitance to the ground. The transmission of the RLC circuit depends on the resistance of the NIS junction described as a resistor R, which depends on temperature.

2.3 Semiconducting InAs nanowires

The InAs nanowires studied in this thesis are III-V semiconductors, with a radial size around 70 nm and length of several micrometers. The wire-shaped quasi-one-dimensional geometry is an important factor for the properties of nanowires which are different from the bulk material [28]. To embed semiconductor nanowires in different devices, it is important to be able to contact them with metals. Due to the Schottky barrier in the interface of many semiconductors and metals, the contact is hard to make transparent. However, in InAs wires, there is an electron accumulation layer on the surface, which results from the pinning of the Fermi level on the surface [29, 30]. Highly transparent ohmic contacts to the wire are thus rather easy to make. Other properties of InAs nanowires include a small effective electron mass which results in high electron mobility, a small direct bandgap, and strong quantum confinement effects.

2.3.1 Electron-phonon coupling of InAs nanowires

The electron-phonon interaction is an important mechanisms regarding to the temperature relaxation of an electron system in a metal or semiconductor. Previously, the electron-phonon coupling in InAs nanowires has been investigated by measuring the electron temperature of the wire using supercurrent thermometry [31]. The supercurrent can flow between two superconducting electrodes placed on top of a nanowire based on the proximity effect. Josephson junctions with InAs nanowire as a weak link have been fabricated both with superconducting terminals made of Nb [32] and Al [33].

The magnitude of the supercurrent in these devices can be modified by changing the distance between the superconducting electrodes. On top of that, the supercurrent can be controlled also by heating the wire and thus increasing the electron temperature.

The measured structure in Ref. [31] was similar to the one shown in Fig. 3.5a. Two superconducting electrodes were placed on top of the wire with direct ohmic contacts and a distance of 60 nm between them. At the ends, the wire was contacted with normal metal electrodes that could be used to control the energy distribution of the electrons, i.e. to heat the electrons in the wire.

The measured critical currents were as large as 350 nA at 370 mK with zero heating voltage. When the temperature was increased to about 1 K, the critical current disappeared. The supercurrent can be suppressed also by applying voltage across the normal metal electrodes at the ends of the wire and thus heating the wire. Comparing the temperature dependence of the critical current and the evolution of the critical current as a function of the heating bias voltage, one can extract the power needed to heat the electronic system by certain amount. From that, the electron-phonon coupling can be calculated. In Ref. [31], the heat flow between the electrons and phonons was assumed to be of the form $Q = \Sigma(T_e^5 - T_{ph}^5)$, and the phonons in the nanowire and substrate were assumed to be well coupled. The electron-phonon coupling constant was found to be $\Sigma = 4.7 \cdot 10^9 \pm 0.3 \cdot 10^9$ W/K^{5}M^3, which is close to the values for typical metallic films [21].

2.3.2 InAs nanowire growth

Many nanowire growth mechanisms used today are based on the vapor-liquid-solid (VLS) method, that was demonstrated already in 1964 by Wagner and Ellis at Bell Laboratories [34]. They used an Au particle as a catalyst for the crystallization of Si from the surrounding vapor. The Au particle was heated so, that it formed an Au-Si liquid alloy on a Si wafer, and the wire grows under the Au-Si droplet.

InAs nanowires were fabricated already in the 1990s by molecular beam epitaxy [35].The source materials, In and As, are heated until they evaporate, and a beam of these particles is directed to a growth wafer which has small Au particles on it. When the nanowire materials (In and As) are streamed towards the chip, the gold particles catalyse the crystallisation of the materials and they condense and form an InAs crystal. The InAs lattice is grown layer by layer and only under the Au particles, and thus wire-shaped structures are formed. With molecular beam epitaxy, it is possible to create very pure, impurity and stacking-free crystal structures. This method is used to grow the wires used in this thesis, by Peter Krogstrup *et al.* at

Niels Bohr Institute, University of Copenhagen [36].

The functionality and performance of the electrical devices involving nanowires depend often on the interface between a semiconducting nanowire and metal electrodes. For example, in the study of Majorana modes in proximity-induces nanowires, it was shown that a soft superconducting gap inducing decoherence in the system is due to the disorder in the interface [37]. Recently, a new method for epitaxial growth of Al on the surface of the nanowire has been developed [36]. Al is deposited around the core with molecular beam epitaxy by rotating the InAs wire during the Al growth. The epitaxial interface between the InAs core and the Al shell is very clean and free of dislocations. The resulting Al shell can be as thin as few nanometers.

Chapter 3

Research methods

Reaching low temperatures is a key factor in being able to operate many nanoelectronic devices. This Chapter introduces first briefly the cryogenic methods used in the experiments. This includes the basic operation principles of dilution refrigerators. After that, a detailed description of the device fabrication is presented. During the whole master's project, a great deal of time and effort was used to develop the recipes and methods for the device fabrication. Even small variations in the fabrication destroyed the operation of the devices. The target is to develop fabrication procedures that would be reliable and repeatable. Finally, I go through the measurement techniques and setups for the low temperature measurements.

3.1 Cryogenic methods

Many experiments in the field of nanoelectronics and quantum technologies require extremely low temperatures, well below 1 K, to reduce the external noise and to prevent thermal energy to wash out the effects one wants to study. Low temperatures are especially needed to achieve superconductivity in different materials. There exists various different cooling methods to reach such temperatures [38]. A short description of the helium dilution refrigerators used in this work is given below.

^{3}He-^{4}He dilution refrigeration was invented already in the 60's [39] but is still the only continuous cooling method that allows to reach temperatures below 300 mK [38]. The cooling power is based on the heat of mixing of two helium isotopes, ^{3}He and ^{4}He. The mixture of these two isotopes has some very bizarre properties that can be seen in the phase diagram in Fig. 3.1. Above 867 mK the two isotopes form a mixture, which depending on the concentration of ^{3}He is either superfluid or normal liquid. However, at lower temperatures, the liquid is separated into two different phases, one with higher ^{3}He and the other with higher ^{4}He concentration. When the

temperature approaches zero, the ^{3}He-rich phase becomes pure ^{3}He. However, in the other phase, the concentration of ^{3}He saturates to 6.6%. The cooling in the dilution refrigerator takes place in the mixing chamber, when ^{3}He atoms from the pure phase move across the phase boundary to the dilute phase. This can be understood by considering the enthalpy H in the two phases. The enthalpy is larger in the dilute phase, and the resulting cooling power can be written as

$$\dot{Q} = \dot{n}_{^3He}[H_d(T) - H_c(T)], \tag{3.1}$$

where $n_{^3He}$ is the molar flow rate of ^{3}He and $H_{d/c}$ is the enthalpy in the diluted/condensed phase.

The continuous circulation is achieved by taking the dilute mixture out of the mixing chamber and leading it to the still, where ^{3}He evaporates, since its partial pressure is much greater than that of ^{4}He. The almost pure ^{3}He gas is then pumped out of the cryostat and fed back to the condensing line, where it cools down and liquifies at the precooler stages of liquid helium, 1K pot and heat exchangers, and finally goes back to the mixing chamber. The cycle for the ^{3}He circulation is thus closed.

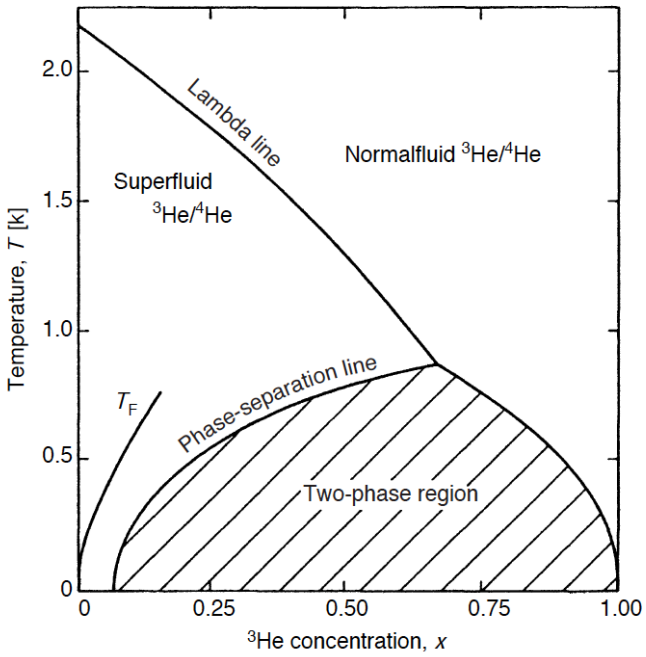

Figure 3.1: The phase diagram for the mixture of ^{3}He and ^{4}He. At temperatures below 867 mK, the mixture separates into two different phases. When the temperature approaches zero, the ^{3}He concentration in the other phase saturates to 6.6%. [38]

In ordinary cryostats, the precooling of the ^{3}He is done with liquid ^{4}He bath at

4.2 K and 1.5 K. However, recently a new cryogen-free method has made it possible to operate a dilution refrigerator without liquid helium as a pre-cooler. Instead, a pulse tube cryocooler can be used to cool down the ^{3}He before pumping it to the mixing chamber. Both ordinary and cryogen-free dilution refrigerators were used in the measurements for this thesis.

3.2 Sample fabrication

The purpose of this work was to measure the thermal properties of semiconducting InAs nanowires. The nanowires were contacted with superconducting electrodes made of Al, either by ohmic contacts or by forming an insulating tunnel barrier. Contacting a semiconductor nanowire is a non-trivial problem, since first one has to remove the native oxide on the nanowire which can also affect the nanowire structure itself. Also, one has to get the metal sticking to the semiconductor properly to obtain low contact resistance. Various different methods for contacting have been created. In the following, the fabrication processes for both the devices with tunnel contacts and with ohmic contacts are described in detail.

Depositing the wires on a marker chip

The nanowires have been grown on separate growth chips, where they stand as a forest of wires, as shown in Fig. 3.2. They are transferred from the growth chip to the marker chips, where the metal contacts are fabricated afterwards. The marker chips consist of 40 bonding pads for the wiring to the sample box and a rectangular area with pre-defined golden alignment markers that allow locating the wires after deposition. A scanning electron microscope image of a marker chip is shown in Fig. 3.3. The markers are triangle and square-shaped, and every combination of four neighbouring markers is unique and makes it possible to determine the location of the nanowire from an image consisting four markers. An array of these marker chips is fabricated on a highly-doped four-inch Si wafer with 200 nm of silicon oxide on top. The larger wafer is then cleaved to approximately 5x5 mm chips, on which the devices are fabricated. Before the wire deposition, the chips were cleaned with the following recipe:

- 2 min in acetone in ultrasonic bath
- rinse with isopropyl alcohol (IPA)
- blow dry with N_2.

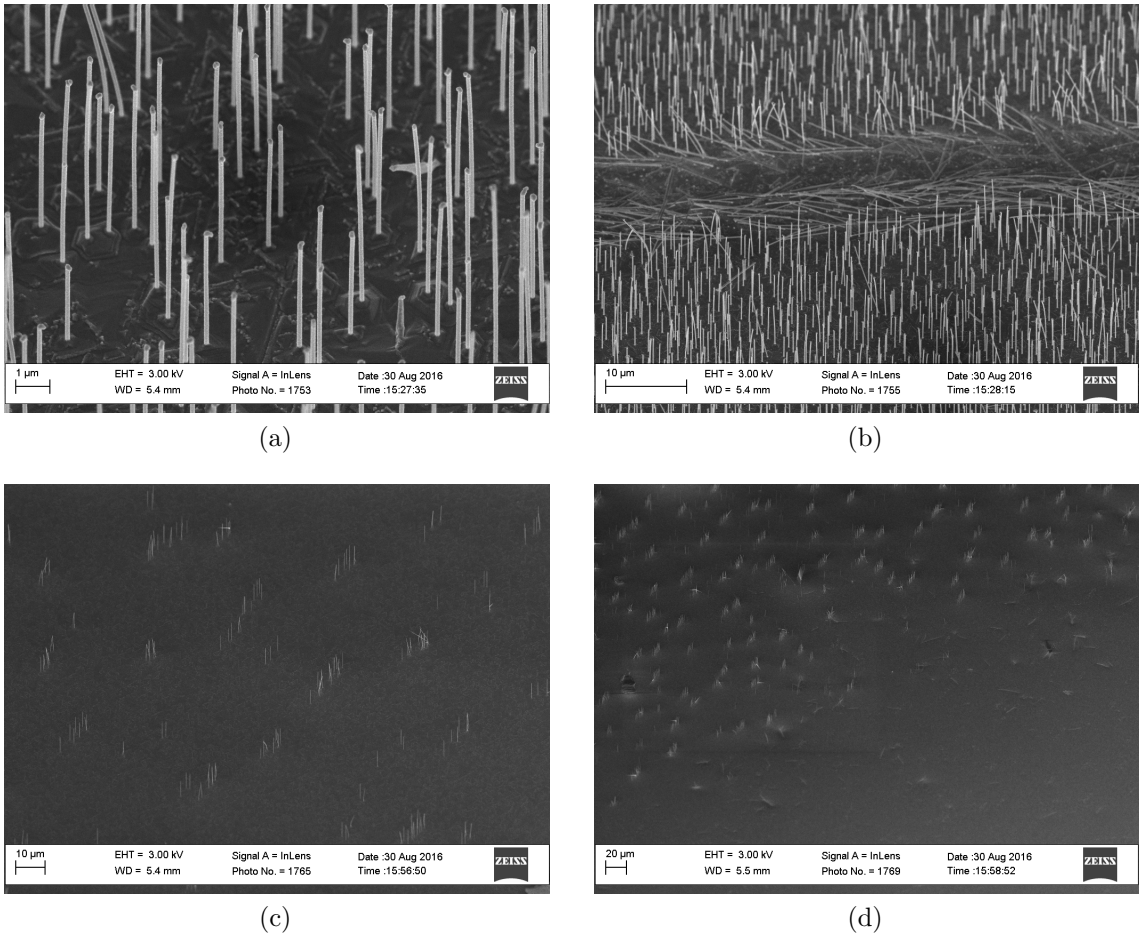

Figure 3.2: a) A forest of wires on a dense growth chip. b) The growth chip is swept with a piece of cleanroom paper in order to transfer the wires to another chip. c) On this chip, the nanowires are grown sparsely. d) The sweep with a piece of paper has to be stronger with a sparse growth chip.

In this work, the wires were transferred by a dry deposition method. One simply takes a small triangle-shaped piece of cleanroom paper with tweezers and touches the growth chip gently with its corner. Some nanowires stick to the paper piece and can be transferred to the marker chip by touching it with the paper. The density of the nanowires vary on growth chips depending on the batch, and this has to be taken into account when depositing the wires. Images of the wires on a growth chip are shown in Fig. 3.2. If the wires have been grown densely, one has to touch the chip with the paper very gently, otherwise the marker chip becomes too full of the wires and it becomes hard to define the rest of the structure. On the other hand, if the nanowires are grown sparsely on the chip, one needs to do even a sweep with the paper, and touch many times the marker chip to get enough wires transferred.

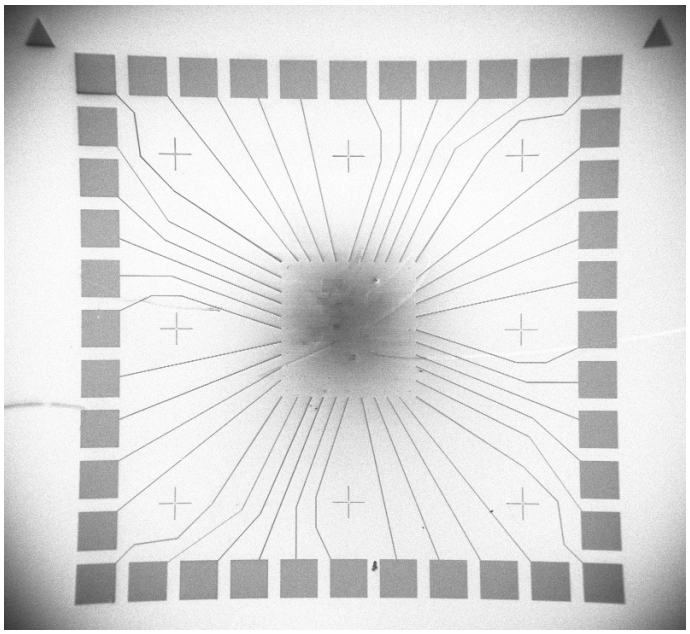

(a)

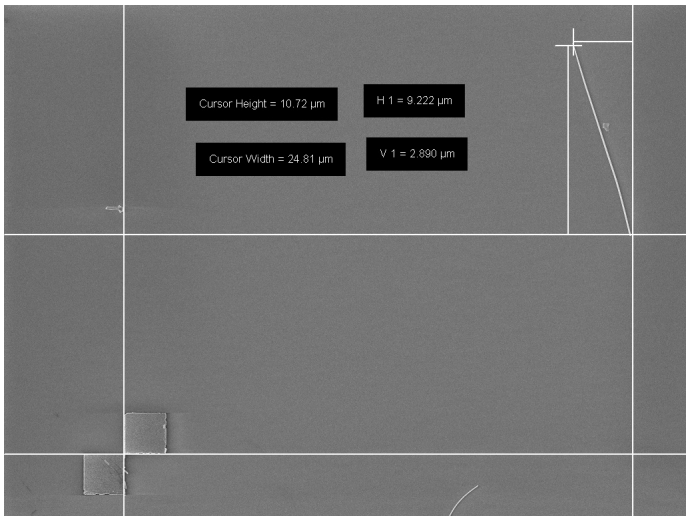

(b)

Figure 3.3: a) A SEM image of the marker chip. On the sides there are 40 bonding pads, from which a few micrometer wide contacts are led to the center. In the middle is the area with alignment markers, where the nanowires are deposited. b) The location of the nanowires is measured with respect to the pre-defined alignment markers, and the exact location of the wire on the chip is thus known.

Locating the wires

The coordinates of the nanowires on a marker chip need to be known, in order to position the electrodes correctly. Once on the marker chip, the wires are located with a scanning electron microscope. The positions of the ends of a wire are measured

relative to a pre-defined marker on the chip, as shown in Fig. 3.3b.

How to proceed from this point depends on the desired structure. If the wire needs to be etched chemically, two rounds of electron beam lithography (EBL) are required: one to make a mask for the etching and another for the metallic structure. Only one round of lithography is required if there is no need for etching. In the following, four different methods to make contacts to the nanowires are described – two for tunnel junctions and two for ohmic contacts.

3.2.1 InAs nanowire with ohmic contacts

The first method to make ohmic contacts is to make direct contacts to the semiconductor. To achieve a good ohmic contact directly to the nanowire, the oxide layer covering the nanowire has to be removed without destroying the nanowire itself. Another way is to use Al-covered wires and make a contact to the Al shell. With Al-covered wires, the interface between the nanowire and the shell is already very clean, and a transparent contact is easier to achieve. The latter process, however, requires wet etching for some parts of the wire (the device structure is explained later) and that makes it more complicated.

Contacts to a nanowire without Al shell

Let us first consider the bare wire. The steps of the facrication process described below is illustrated in Fig. 3.4a. The Al electrodes are defined by the electron beam lithography. A double layer structure for the mask is made of copolymer (MMA) and poly-methyl-methacrylate (PMMA). Two layers are used not to achieve the undercut for multi-angle evaporation but to help the lift-off at a later stage. The resist is spinned on top of the chip with the following parameters:

- Spinning MMA: 2500 rpm, 60s
- Spinning PMMA A4: 4000 rpm, 60s
- Baking: 160 °C, 5min

After that, the resist is exposed to an electron beam and developed in Methyl Isobutyl Ketone (MIBK) solution with one part of MIBK and three parts of IPA.

Once the mask is created, the electrodes can be deposited with evaporator. To make good transparent contacts, the native oxide on the surface of the wire has to be removed without destroying the nanowire itself. Several methods for that have been developed, such as wet etching and sulfur passivation [40]. In this work, Ar

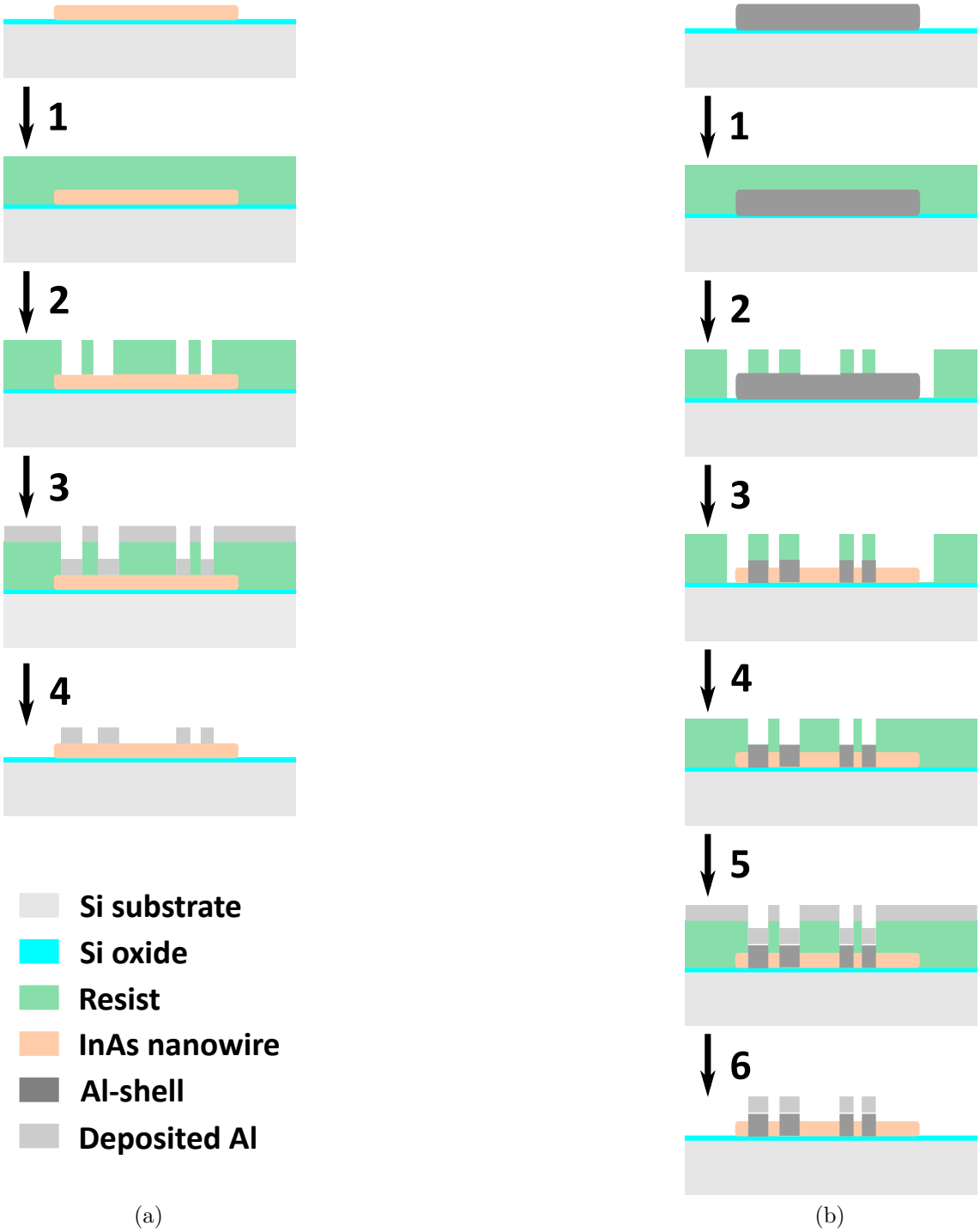

(a) (b)

Figure 3.4: The fabrication steps for the device with clean contacts to a bare nanowire (a) and for a nanowire with Al shell (b). a) 1: Spinning of the resist. 2: EBL and resist development. 3: Ar plasma for removing the native oxide of the nanowire and metal evaporation. 4: Lifting off the resist and metal on top of it. b) 1: Spinning of the resist. 2: EBL and resist development. 3: Etching the Al shell. 4: Spinning new resist, EBL and development. 5: Removing the native oxide from the Al shell, controlled oxidation if making tunnel junctions and metal evaporation. 6: Lifting off the resist and metal on top of it.

plasma etching was used. The plasma gun is installed in the evaporation chamber, and the evaporation can be done immediately after the etching in the same vacuum without exposing the sample to the air. The plasma etches easily also the actual nanowire, and one has to be sure not to etch too much. In Ref. [33], a good contact for sustaining supercurrent was achieved by etching one third of the wire away. For the electrodes, a 5-nm-thick Ti sticking layer was deposited before evaporating 100 nm of Al. The resist was lifted off with acetone. The resulting device is shown in Fig. 3.5.

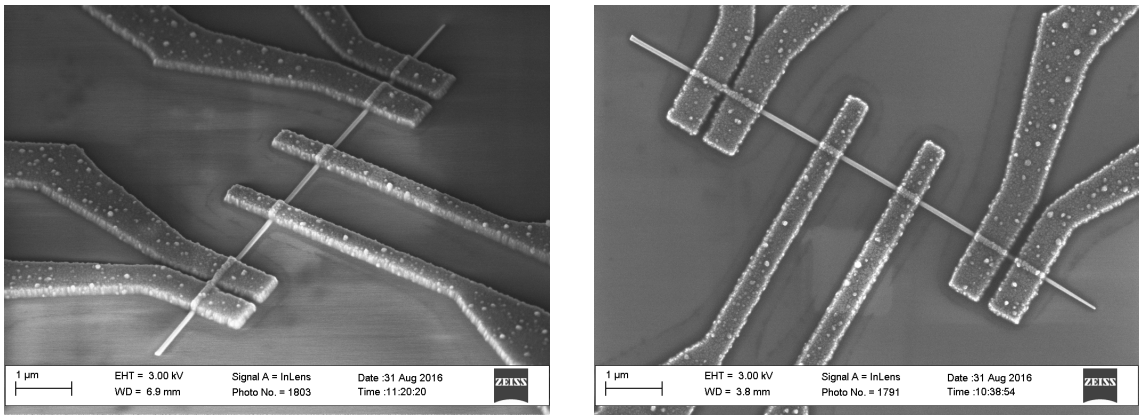

(a) (b)

Figure 3.5: a) A tilted-angle SEM image of the measured device with a bare InAs nanowire and Al electrodes. The pairs on the sides are used as a supercurrent thermometer, and they have a distance around 100 nm between the electrodes. The two electrodes in the middle are used as a heater to raise the electron temperature on the wire through Joule heating. b) A top view of the wire with two thermometers (with different gap length) and a heater in the middle. The minimum distance achieved between the electrodes was around 50 nm.

Contacts to a nanowire with Al shell

Another way to make transparent ohmic contacts is to use nanowires covered with Al shell. The epitaxial Al shell makes a very good contact with the semiconductor lattice, and metal-metal contacts are easy to fabricate. The downside of this method is that it requires wet etching for removing the Al between the contacts, which makes the process harder to realize and also more time-consuming due to multiple lithography rounds.

The following steps are illustrated in Fig. 3.4b. For the etching, one has to define a mask with similar methods as explained above for the metal deposition. However, the undercut in the resist is now not desired, since then a larger part of the wire than desired would be exposed to the etchant. One layer of PMMA is enough to

make a good etching window. After the mask is created, the chip is immersed in MF-CD-26 and after certain time cleaned in distilled water (DIW). The timing at this point is very crucial because the etching of the native Al oxide is much slower than the etching of the aluminum. In the fabrication recipe used for this thesis, it took around 65 s to etch through the oxide, but only couple of seconds to etch the aluminum. If the etching is not stopped, it continues along the wire under the resist, and easily removes the Al shell from the distance of the whole wire. The etching is stopped by flushing the chip in two beakers of DIW (90 s+30 s). After etching, the resist is removed with acetone and the chip is cleaned with IPA.

The etching procedure is not very precise, and the reason for that is not completely known. The wire is not etched only in the perpendicular direction, but the chemical acts also along the wire, resulting in overetching. The distance for that varies from time to time, and even on the same chip for different wires. That has probably to do with the way how the resist is stuck on the chip and the wires of top of it. Also the used resist and the fabrication parameters, such as the baking temperature and time, could affect the overetching rate. In table 3.1, overetching lengths have been listed for five different wires on a same chip, etched at the same time. There is a variation from 300 nm to as long as 600 nm of overetching which makes it difficult to etch small segments precisely.

Of the other etchants, at least Transene D has been used succesfully to achieve even better results with respect to the etching resolution [41]. However, it requires a big effort to develop a working recipe with a new chemical, which is why there was no time to test it for the purpose of this thesis.

Table 3.1: This table shows the overetching for one particular fabrication round. Five nanowires were deposited on the same chip. The wires had multiple etching windows for the electrodes. The draw length corresponds to the length of the etching window along the wire, and etch length is measured after the actual etching. The overetching varies a lot even between the wires on the same chip. For the wire 5, the whole Al shell was gone.

Wire	Draw length	Etch length	Overetch
1	1100	1700	600
1	500	1000	500
2	830	1200	370
2	500	800	300
3	720	1200	480
3	1250	1600	350
3	500	830	330
4	280	750	470
5	1150	> 2350	> 1200

After etching, it is good to image the wire with SEM to see the results. Then, a new round of lithography is needed to fabricate the electrodes on top of the wire. That is done similarly as explained above for the device with direct contacts to the nanowire. The native oxide on the surface of the Al shell has to be removed with the Ar plasma in the evaporator, and after that Al electrodes can be deposited.

3.2.2 InAs nanowire with tunnel contacts

Tunnel contacts can be made both to an Al-covered nanowire and also to bare wires. For the first case, the fabrication process shown in Fig. 3.4b. The etching is done similarly as in the case of making ohmic contacts. The aim is to etch the parts of the wire where the electrodes are not deposited, in order to decrease the proximity effect in the nanowire and force the current to flow through the nanowire, not only through the Al shell. If the nanowire is too proximised by the Al shell, the measurement does not anymore provide information about the electron temperature in the nanowire itself. After etching, another lithography is made for the metal deposition. To make the tunnel junctions, one has to oxidise the epitaxial Al shell on the wire. First, one has to remove the native oxide by Ar plasma etching and then perform a controlled oxidation in the evaporation chamber, followed by the evaporation of Al (100 nm).

The tunnel junction to the bare InAs wire is made in two different lithography and evaporation steps. First, a thin layer of Al (5 nm) is evaporated through a mask defining the positions of the electrodes on the wire. To make the wire covered not only from the top but also from sides, the evaporation can be performed in multiple angles (e.g. $-5°, 0°, 5°$). Then another lithography is performed to create the mask for the electrodes. The tunnel junction is made by oxidising the thin aluminum layer, and after that another layer of Al for the electrodes is evaporated.

3.2.3 Measurement setup

The measurements were performed in a dilution refrigerator with a base temperature around 50 mK. The construction of the cryostat is described in detail in Ref. [42]. The sample is glued to a brass sample holder with vacuum grease and bonded with Delvotek 5332 wire bonder using 25-µm-thick Al wire. The printed circuit board at the sample holder has 12 pads which are connected to the DC measurement lines in the cryostat. After attached to the cryostat, the sample holder is closed with a threaded brass cover to reduce the noise caused by the electromagnetic radiation coming from the 4.2 K environment. Microwave noise is filtered also with Thermocoax cables, that are used between the sample holder and the connector box at the room

temperature.

The bonding of the nanowire samples turned out to cause a lot of problems at first. Many times, the wires were blown up between the electrodes that were bonded. A possible reason for that could be the static electricity in the needle or insufficient grounding of the user while bonding. Another problem with the bonding arose when the bonding parameters were too harsh, and the boding pads broke such that they became shorted to the doped substrate. As conclusion, one has to take good care of the grounding in order not to break the wires and determine gentle enough bonding parameters.

Two different measurement setups were used for the measurement of the nanowire devices. The devices with tunnel contacts were measured in voltage bias by applying a known voltage between the electrodes and measuring the current (Fig. 3.6a). The supercurrent in the devices with ohmic contacts was measured in current bias because with the supercurrent there is no voltage difference across the junction (Fig. 3.6b). When the critical current is achieved, the device switches to a normal state and a voltage difference. The schematics in Fig. 3.6 show also the device layout, which consists of the nanowire, two electrodes for the heater to increase the electron temperature in the wire by Joule heating, and two to be used as a thermometer.

The main instruments used in the measurements were voltage sources, amplifiers and digital multimeters. A voltage bias was created with a floating voltage source Agilent 33220A function waveform generator and isolated voltage source Stanford Research Systems SIM928. The desired voltages for the measurements were in the range of millivolts and to obtain that, a voltage division is needed. The voltage divider was created with a resistor network after the voltage source. The current bias was achieved by inserting a large resistor in series with the voltage source and the sample. The voltage signals were amplified with preamplifiers (Femto's DLPCA for current and DLPVA for voltage amplification) and recorded with Agilent 34401A digital multimeter.

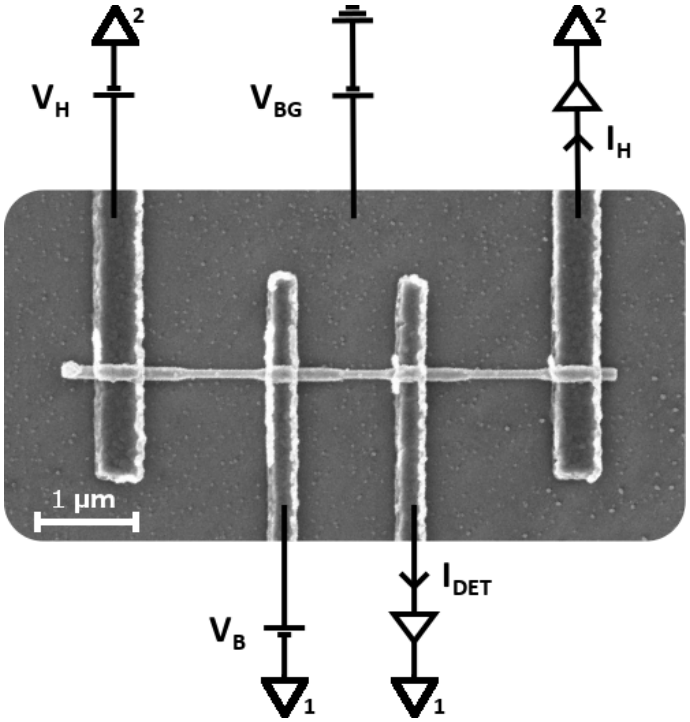

Figure 3.6: a) The measurement setup for the voltage-biased measurement used with the tunnel junction devices. The electrode pair in the middle was used as a thermometer and the outer pair as a heater. The junctions were biased from the other side with the bias voltage for the thermometer, V_B, and the heating bias V_H. The detector current I_{DET} and heating current I_H were measured with amplifiers and recorded with a digital multimeter. The doped substrate was used as a back-gate for the device by applying a gate voltage V_{BG}. b) The setup for the current-biased 4-point measurements. The junction on the left was current biased, and the voltage across the junction was measured. The two electrodes on the right were used to heat the device.

Chapter 4

Results

The goal with the experiments was to measure the electron-phonon coupling of InAs nanowires. The idea was to heat the wire by Joule heating, i.e., by applying current through the wire with two electrodes. Another pair of electrodes is used for thermometry. This thermometer is first calibrated against the bath temperature, after which it can be used to detect the electron temperature during the heating of the wire. A global back-gate is used to tune the conductivity of the semiconducting nanowires.

The first approach for this was to make tunnel contacts to the nanowire, as described in the fabrication section above. If the junctions between two electrodes would behave like a SINIS structure, they could be used to measure the temperature of the normal part. There were difficulties in the measurements using this method, and another scheme was tried after that by measuring the supercurrent through the wire in a SNS junction. Results from these both experiments are presented in the following.

4.1 Heating experiments with tunnel junction thermometry

The first measurements were performed with InAs nanowires contacted with tunnel junctions. The junctions were made by oxidizing Al shell on top of the wire and after that evaporating the Al electrodes on top of the oxide. Before evaporation the shell was etched between the contact areas. The device layout is shown in Fig. 3.6a.

In order to make the nanowires conductive, the chemical potential needs to be in the conduction band. For the InAs wires in these experiments, this was obtained by applying a gate voltage to the conductive substrate under the nanowire, which

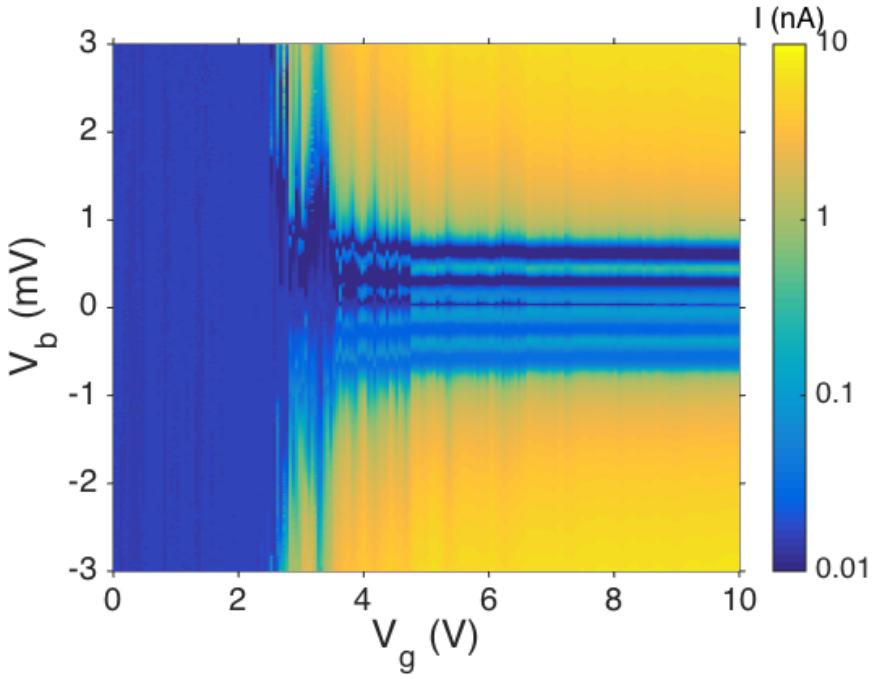

Figure 4.1: The gate voltage dependence of InAs nanowire with tunnel junctions to the Al-shell. The current is shown as a color with respect to the gate and bias voltages. This picture shows the transition of the nanowire from non-conductive to conductive state when applying gate voltage.

works as a global back-gate. This affects the whole nanowire, not only some part of it. The gate-dependence for the SI(NW)IS junction between two electrodes with an etched segment in the middle is shown in Figs. 4.1 and 4.2. The required gate voltage for making the wire conductive with the back-gate was between $2-3$ V. At roughly $V_{bg} = 5$ V, the I-V characteristics stabilized, and increasing the gate voltage further had only a minor effect on the behaviour.

In Fig. 4.2 one can see also the gap in the I-V curve resulting from the two tunnel junctions in series. In this case, the edge of the gap is around 800 μV. The energy gap in Al is approximately 200 μV, which implies that the junction between the nanowire and the electrode is more like SIS type rather than NIS. In S_1IS_2 junctions with two different superconductors, the gap edge corresponds to energy $2(\Delta_1 + \Delta_2)$, where Δ_1 is the energy gap of superconductor S_1 and Δ_2 of superconductor S_2. The Al cover on top of the nanowire proximises the nanowire, which has also an energy gap close to that of Al in this case.

Fig. 4.2 shows also a peak approximately in the middle of the gap around $V_b = 400$ mV. That could arise in a junction between two different superconductors and would correspond to the energy $\Delta_1 - \Delta_2$. In this case, however, the Δ in the nanowire should be close to the Al gap, and the difference $\Delta_1 - \Delta_2$ should be closer

to zero voltage, not at $V_b \approx 400$ μV. A more feasible reason for the peak could be that the other junction switches to the normal state and thus the peak occurs in the middle of the gap.

The thermometer has to be calibrated against the bath temperature before using it to detect the Joule heating of the wire. In Fig. 4.3 one can see the temperature dependence of the I-V characteristics of the SI(NW)IS junction for an etched wire, like in Fig. 3.6a. There is a clear temperature dependence when the temperature is increased to over 600 mK. However, at $T_{bath} < 300$ mK, the dependence becomes quite weak.

I have measured also an unetched InAs wire, covered with a full Al shell. The I-V characteristics is seen in Fig 4.3b. The supercurrent at low V_b (the steep slope) is not as smoothed as for the etched case, and there is a larger temperature dependence. The peak in the middle of the gap is sharper. The overall form, however, is quite close to the etched case, which indicates also that the behaviour of the etched wire was close to that of Al.

For the intended use in a single-photon detector, the temperature sensitivity should remain good below 100 mK. The sensitivity for the unetched wire was measured in constant voltage bias by changing the bath temperature and measuring the current between the thermometer electrodes. This dependence is shown in Fig. 4.4. One can see two different slopes there with a crossover at around 350 mK.

Experiments were also performed to measure the response to the heating with the unetched InAs wire in order to demonstrate the heating and detection of the response. The nanowire was heated with the outer pair of electrodes by applying a heating voltage. The voltage was applied with a function generator that produced V-shaped cycles from 1.5V to -1.5V, applied through a voltage divider with 1/1000 division. The current was measured with the two thermometer electrodes in the middle of the wire, with different constant bias V_b. The measured current for $V_b = 0.15, 0.6$ mV is shown in Fig. 4.5. The curve in Fig. 4.5a shows heating peaks around $V_{heat} = 0$ and in the middle of the positive and negative side of the gap, as expected from the I-V characteristics shown before. With some bias V_b, there was also cooling provided by the heater electrodes. That is seen as peaks down to negative values in Fig. 4.5b.

These measurements with the tunnel junction devices demonstrated the principle for the heating measurement. When the heating power is known, one could in principle calculate the electron-phonon coupling if the thermometer current would be calibrated against the bath temperature. However, the problem with the SI(NW)IS-thermometer, where nanowire behaves like a superconductor, is that the I-V characteristics do not depend only on the temperature of the wire but also on the temperature of the Al

parts. When the thermometer is calibrated by changing the bath temperature, also the temperature of the Al changes and the calibration is not correct. The heater used in the actual heating measurement would only heat the nanowire, and the thermometer could not be reliably used to detect its electron temperature. With a SNS thermometer instead, the calibration is not a problem, since under 200 mK, the quasiparticles are not thermally activated and only the supercurrent is sensitive for the temperature change. This will be studied in the following.

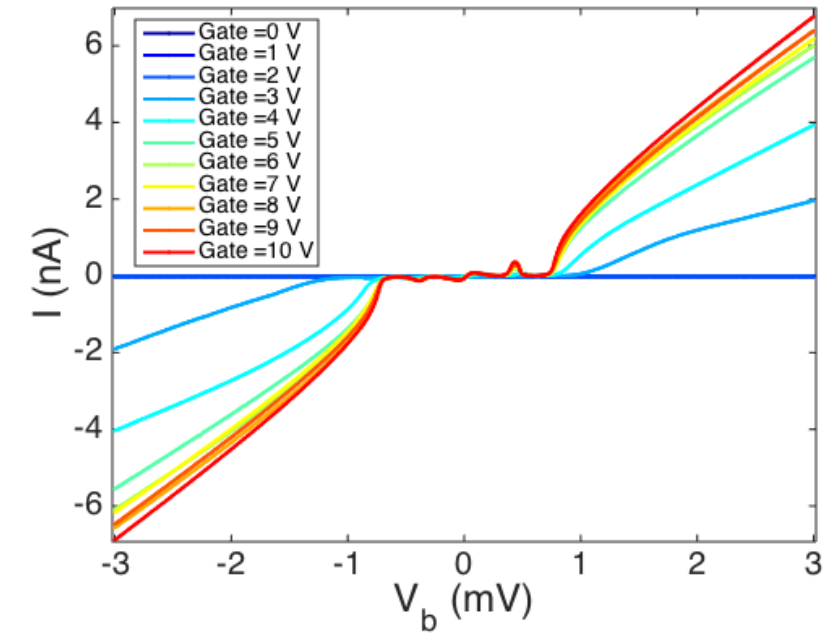

(a)

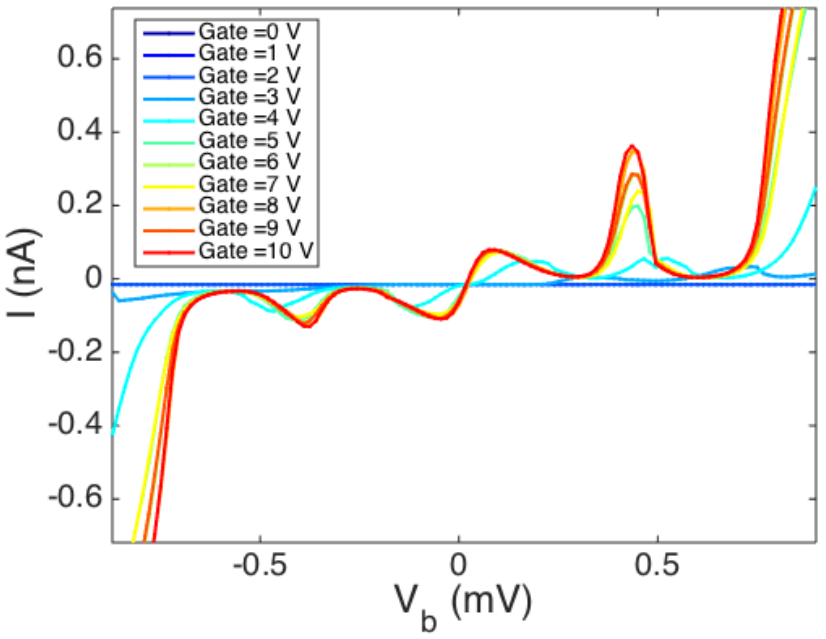

(b)

Figure 4.2: The gate voltage dependence of InAs nanowire with tunnel junctions to the Al-shell. a) The I-V curve is shown for $V_g = 0$ V...10 V. At $V_g = 0$ V,1 V,2 V, the nanowire is non-conductive. At larger V_g, it starts to conduct and saturates around $V_g = 10$ V. b) Zoom to the gap at $|V_b| < 800$ μV. Around $V_b = 0$ V, there is a behaviour related to supercurrent flow. The peaks around $|V_b| \approx 400$ μV are interpreted as a switching of the other tunnel junction. The behaviour of these peaks is hysteretic, which is the reason for the right peak being higher.

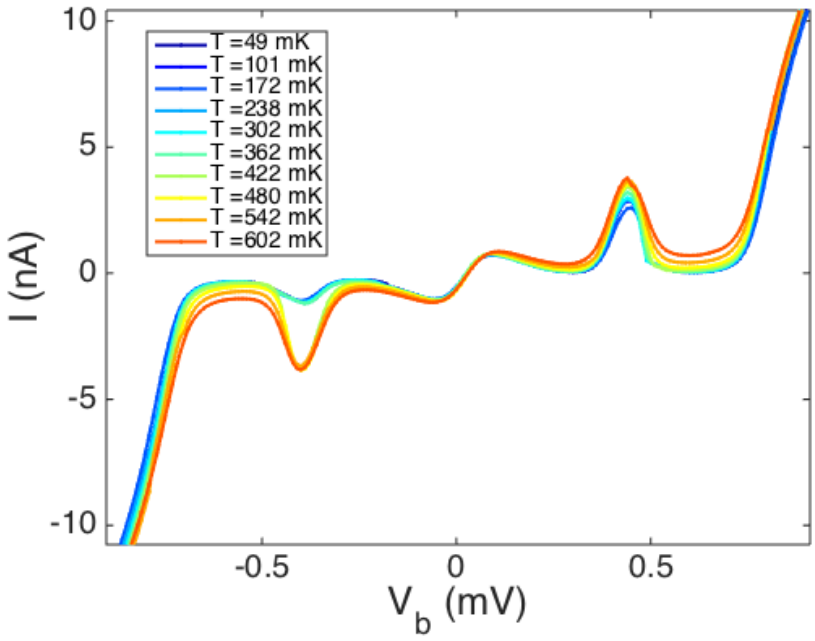

(a)

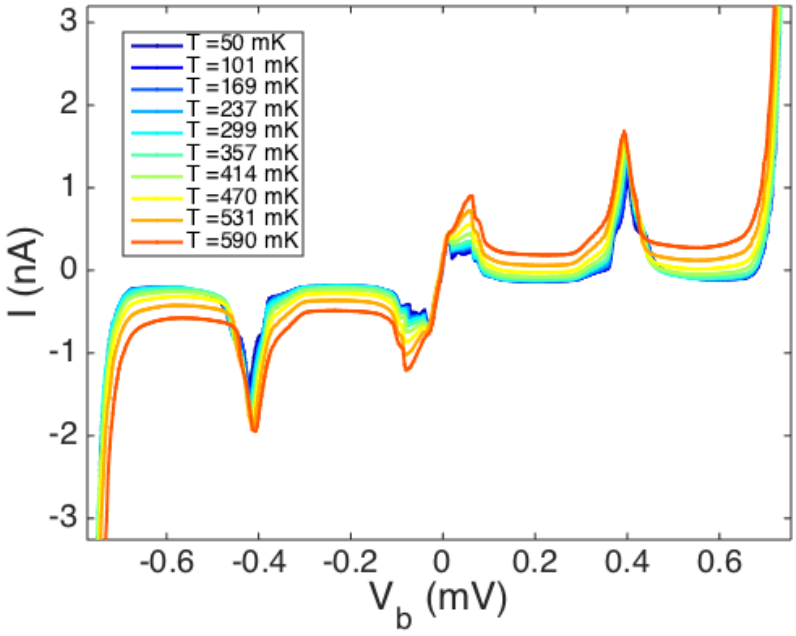

(b)

Figure 4.3: The temperature dependence of the I-V characteristics of a) an etched Al-covered InAs nanowire with tunnel junctions between the wire and the electrodes and b) an unethced Al-covered wire.

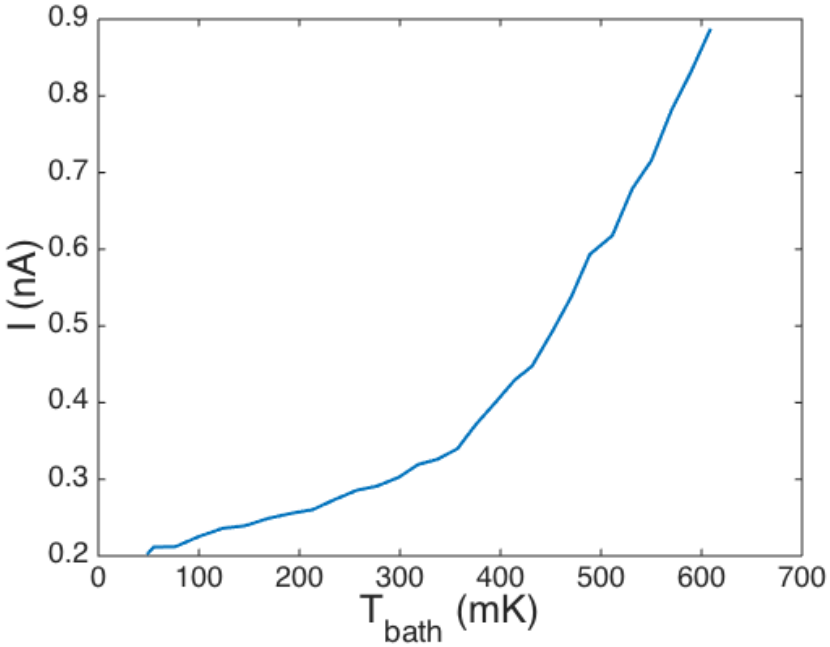

Figure 4.4: The current of an unetched InAs nanowire as a function of the bath temperature at constant bias V_b. Below 350 mK, the dependence becomes weaker.

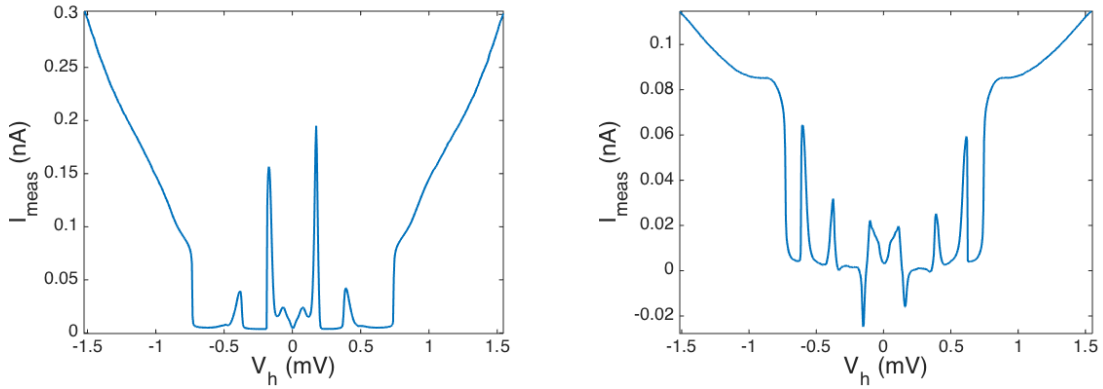

(a) (b)

Figure 4.5: The heating cycles for a) $V_b = 0.6$ mV and b) $V_b = 0.15$ mV. The heating was provided with the outer pair of electrodes, and the current was measured with the thermometer electrodes. The junction with SIS-like nature resulted in complex behaviour with both heating (increased I_{meas}) and cooling (peaks down to negative values) present with some bias voltages.

4.2 Experiments with supercurrent thermometer

After the experiments with the tunnel junction device, another method for measuring the temperature of the nanowire was developed in order to overcome the problems with the temperature calibration. Superconducting Al electrodes are deposited directly on the nanowire to make a transparent ohmic contact. The distance between the thermometer electrodes is kept small enough, so that a supercurrent can flow across the SNS junction. Another pair of electrodes with a longer distance in between was used to heat the wire. The measurement setup for the following experiments is shown in Fig. 3.6b. The devices were measured in current bias.

The supercurrent flow across the SNS junction depends on the interfaces between the Al electrodes and the nanowire. If the interface is not transparent enough, the junction cannot sustain supercurrent. The interface quality depends a lot on the fabrication method. When depositing the electrodes directly on the nanowire, one first has to remove the native oxide from the surfcace. There are different methods to do that, such as sulfur passivation or plasma etching, and the latter was used in this thesis. The etching was done in the evaporation chamber just before the metal deposition. The plasma does not just remove the oxide, but affects easily the lattice of the nanowire as well. In Ref. [33], the best supercurrent was obtained by etching 1/3 of the nanowire in addition to the oxide layer.

The results from the experiments with SNS thermometer are presented in Fig. 4.6. As one can see, there curves do not exhibit any supercurrent, which would be seen as a zero measured voltage V_{meas} below a certain current value. For a device with 10 s etching time, which corresponds to roughly $1/3 - 1/2$ of the wire etched, the behaviour is almost linear, with no sign of the supercurrent. The ohmic behaviour is seen in Fig. 4.6a. The hypothesis after this measurement was that maybe the etching was too powerful and damaged the surface of the nanowire. The plan was to reduce the etching time to obtain a better interface between the nanowire and the electrodes. In Fig. 4.6b, the etching time was reduced to 5s, and there is a sign of supercurrent at low bias currents. The resistance decreases, but does not reach zero as would be in the case of supercurrent. This measurement supported the hypothesis about the etching time affecting the interface quality. However, when the etching was decreased even more both in time and power, the behaviour started to look again more linear as seen in Fig. 4.6a.

Varying the plasma etching time did not lead to an interface which could sustain supercurrent. In Ref. [33], the electrodes were deposited with similar methods as in this work, directly on the nanowire. They have measured succesfully the supercurrent in this kind of device. However, the etching process was different – they used wet

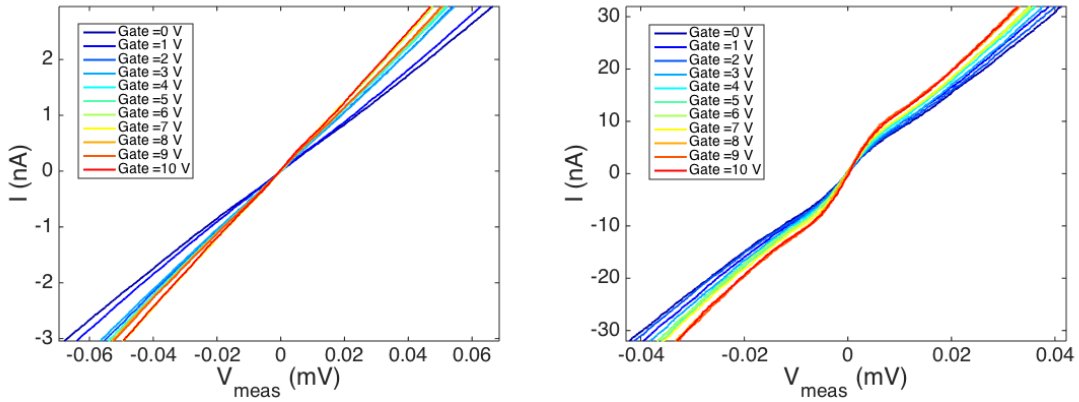

Figure 4.6: a) The I-V characteristics of the SNS junction with different gate voltages for the wire with 2 s of plasma etching time. The behaviour is almost ohmic, since the interface quality is not good enough for supercurrent to flow. An ohmic behaviour was measured also for the wires with an etching time of 10 s or more. b) The I-V characteristics of the SNS junction with different gate voltages for the wire with 3 s of plasma etching time. At small V_{meas}, there is a clear decrease of the resistance, which is a sign of the supercurrent. However, the resistance did not vanish for any device by changing the etching parameters

etching in buffered hydrofluoric acid. This process can affect the nanowire surface differently than plasma etching, and can be the reason for the different behaviour. The short etching times indicate that the plasma etching, in which the surface is bombarded with ions, is more aggressive process for the nanowire than the wet etching. In addition, the fabrication of the nanowires themselves can have differences that affect the nanowire properties.

As the experiments did not show any supercurrent, new methods either for the device structure or the fabrication process had to be considered. One idea was to use Al-covered wires, as in the setup of Fig. 3.6a, but instead of a tunnel junctions make direct ohmic contacts to the shell. The advantage of this method is that the interface between the nanowire and the shell is epitaxially matched [36], and the Al electrodes are easy to deposit and contact to the shell. As a requirement for this kind of structure, one has to be able to etch small segments of the shell between the thermometer electrodes. In Ref. [33], the etched segment varied between 100 nm and 450 nm, and the magnitude of the current decreased from 100 nA with the smallest to 1 nA for the largest lengths. The etching resolution with the method used in this thesis was not small enough - the shorters length was more than 300 nm at best and it varied a lot, as shown before in Table 3.1.

Instead of changing the recipe totally for making new wires by ourself, the experiment continued with the nanowires and devices that were fabricated in the Quantum Transport Group at Delft University of Technology in the Netherlands. These wires were etched with an Al etchant Transene D, and a distance of 50 nm between the electrodes was possible to achieve. The measurement setup was similar to the one shown in Fig. 3.6b, except for the gate electrodes. Instead of using a global back-gate, separate gates were made for each junction.

The following measurements were performed by Libin Wang. In Fig. 4.7, one can see the measured voltage of the thermometer in a current bias. Now there is a clear supercurrent below the switching current, as the measured voltage is zero. In addition to the switching current, one can see also the smaller re-trapping current. Reason for the hysteresis is that in the normal state, the wire is warmed up by the Joule heating causing the wire to switch back to the supercurrent state at lower current values [43]. The calibration of the thermometer is done by sweeping the cryostat temperature and measuring the switching current of the junction. The switching current has a small scatter and is measured multiple times to obtain a histogram of the data, from which a mean is calculated. The data in Fig. 4.8 shows the switching current on the vertical axis with respect of the heating current on the horizontal axis for different base temperatures. The switching current can be converted to temperatures according to the calibration, and the heating current corresponds to certain heating power $P_h = R_{nw} I_h^2$, where R_{nw} is the resistance of the nanowire in a normal state. This is presented in Fig. 4.9. The data is measured at 70 mK base temperature. The fitting is done by using the equation of the form $Q = \Sigma(T_e^2 - T_{ph}^2)$. The exponent is different from that in the Eq. (2.13), which was derived for the metals by using the free electron model. The smaller exponent is reasonable since a nanowire is an one-dimensional object, which affects to the heat capacity.

The preliminary results prove that the supercurrent thermometry with a SNS junction can be utilised with Al-covered InAs nanowires to determine the electron temperature in the nanowire. The etching with this method requires small resolution, which can be obtained with the right fabrication recipe.

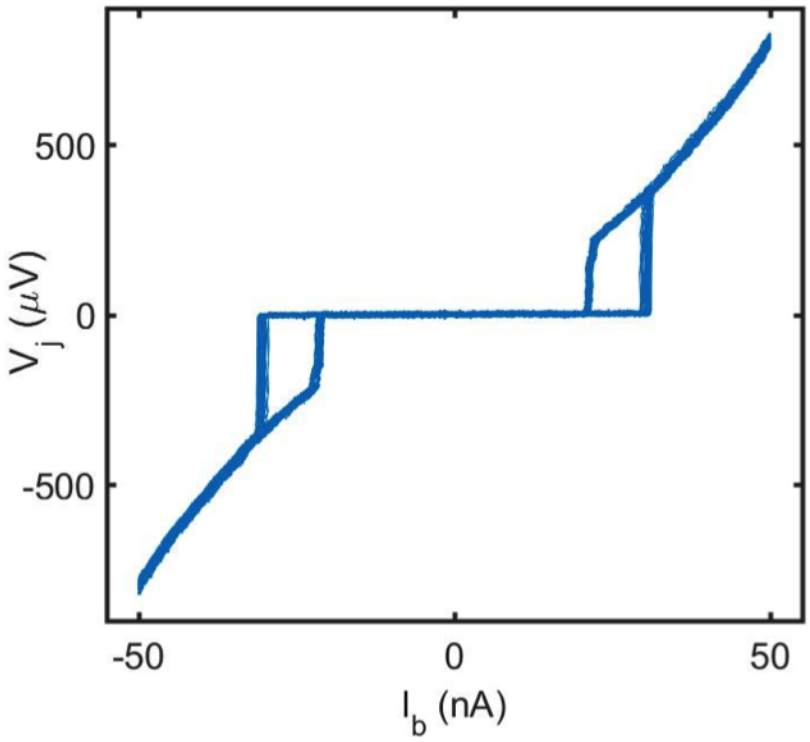

Figure 4.7: The supercurrent measured across a SNS junction, with a segment of InAs nanowire between the superconducting electrodes. The voltage V_j was measured for the applied I_b. Below the swtiching current, the voltage remains zero. The behaviour is hysteretic, and the re-trapping current is smaller than the switching current.

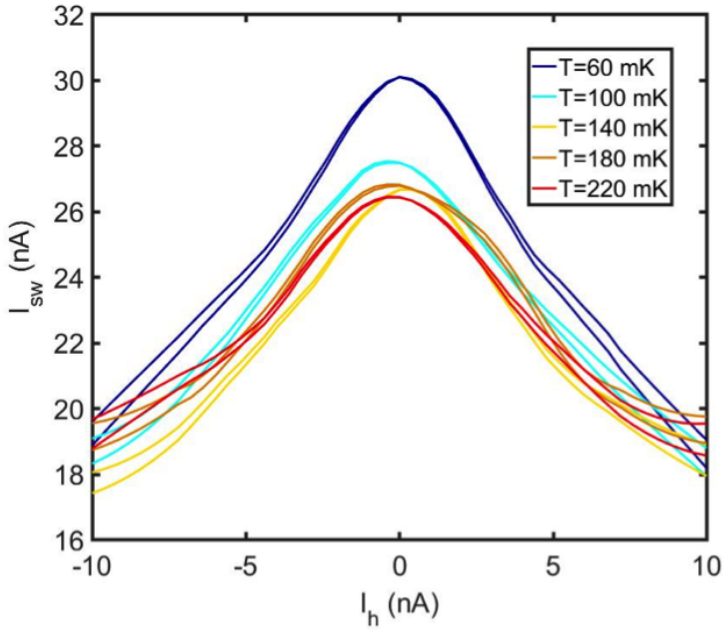

Figure 4.8: The switching current with respect to the heating current for different base temperatures. The switching current has to be calibrated against the bath temperature.

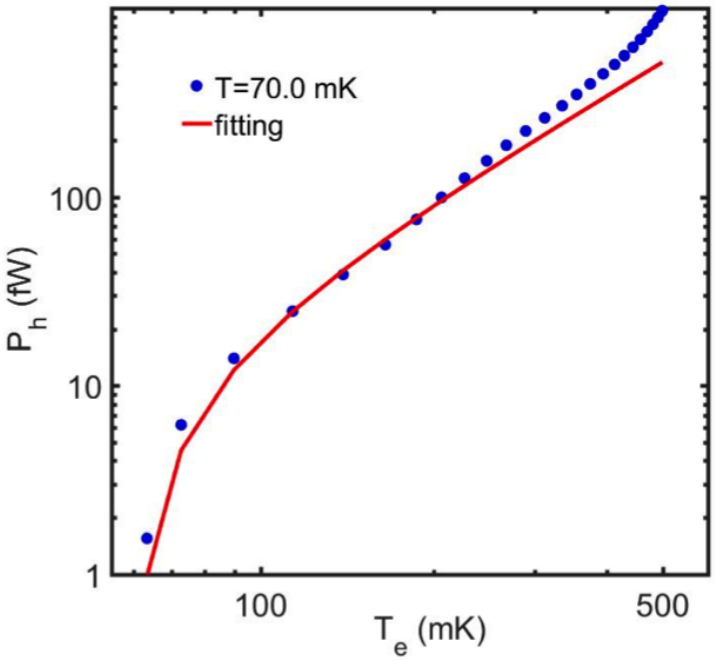

Figure 4.9: The swtiching current is converted to temperature values on the horizontal axis, and the power applied to the nanowire through the heating electrodes is on the vertical axis. The dots represent the measured data at $T = 70$ mK. The red curve is a fit of the form $Q = \Sigma(T_e^2 - T_{ph}^2)$.

Chapter 5

Conclusion

The goal of this thesis was to investigate the strength of the electron-phonon coupling in semiconducting InAs nanowires. The motivation for this study arises from the development of single-photon detector for microwave photons, based on ultrafast tunnel junction thermometry. The working principle of the detector is based on monitoring the temperature of a small metal island which can absorb single energy quanta. The semiconducting InAs nanowires could provide several benefits as an absorber, including the tunability of the semiconductor by gate voltage, smaller electron density and hence smaller heat capacity, and possibly smaller electron-phonon coupling, which would mean longer relaxation time for the temperature of the absorber island.

InAs nanowires were fabricated with molecular beam epitaxy on an InAs chip, on which the wires were grown as "forests" made up of numerous wires standing close to each other. Small portion of the wires could be transferred to another chip with a piece of paper and tweezers, after which single wires could be located and contacted with electrical contacts made by nanofabrication methods including electron beam lithography and evaporation of metals.

The thermal properies of an InAs nanowire can be investigated by measuring the current or voltage over a segment of the wire under certain conditions. In this thesis, two different measurement configurations were used to measure the properties of the nanowire. First, the nanowire was contacted with superconducting Al electrodes with tunnel junctions at both ends of the wire, resulting in a hybrid SI(NW)IS junction. The tunnel junctions were fabricated by oxidising the Al shell covering the InAs wire. Al electrodes were deposited on top of the insulating oxide barrier, and the section between the electrodes was etched in order to get rid of the Al shell. In the other configuration, Al electrodes were deposited directly on the semiconducting nanowire or to the Al shell without an oxide layer, resulting in SNS junction.

In the first measurement setup the difficulty was to prevent the nanowire to become proximized by the Al shell which was required to make the tunnel contacts. If the nanowire is heavily proximised, the electrical measurements over the SI(NW)IS junction do not reveal the properties of the InAs nanowire itself but depend on Al properties instead. This method was investigated in this thesis by measuring the I-V characteristics at different temperatures (50 mK$< T_b <$ 600 mK) but it did not prove to be successful – the junction behaved more like a SISIS junction in which the nanowire did not influence much. The characteristics were what one expects for a plain Al device.

Another major challenge with the experimental work done in this thesis arose from the fabrication. Making the direct ohmic contacts to the nanowire in order to drive supercurrent through it turned out to be difficult. Two different methods for the contacts were tried. In the first method, a thin layer of Ti was deposited on top of a plasma etched InAs nanowire in order to make the metal sticking properly to the semiconducting surface, and then the Al electrodes were deposited on top of that layer. Another method was to use nanowires covered with Al shells and etch the shell away except from the areas where the Al electrodes are deposited. With this method, the contact is easier to make, since the semiconducting nanowire and the shell are already very well matched, and it is easy to make a proper contact to Al shell. However, this requires etching of a nanowire segment in between the electrodes, otherwise the current would flow in the shell and not through the wire. With the first method, the contact did not become good enough – signs of the supercurrent were observed in the I-V characteristics but a proper SNS behaviour was not observed. With the latter method, the difficulty was to etch short enough segments of the nanowire because too long distance would suppress the supercurrent. However, there are various methods for etching, and it has already been acheived to etch small enough segments with a different etchant than the one used in the fabrication of the devices for this thesis project.

The research continues in the PICO group at Aalto University with devices where ohmic contacts are made to the epitaxial Al shell covering the InAs wire. The fabrication of the wires and devices is done in the Quantum Transport Group at Delft University of Technology and subsequent measurements are made at Aalto University. These devices have shown proper supercurrent over the S(NW)S junction. The magnitude of the supercurrent was calibrated against the bath temperature, and then measured as a function of heating power applied to the nanowire. The thermal properties of InAs nanowire can be investigated from these measurements. The first results show a behaviour which follows the equation of the form $Q = \Sigma(T_e^n - T_{ph}^n)$

approximately with an exponent $n = 2$ at $T < 200$ mK, compared to the $n = 5$ dependence with thin films of normal metal. In analysing the results further, one should take into account that there may be a temperature gradient in the nanowire during the measurements.

Investigating the thermal properties of different materials at cryogenic temperatures is an important topic in the field of quantum devices since it opens possibilities to create unique applications in nanoelectronics utilizing quantum phenomena. The feasibility of InAs nanowires for the purpose of single-photon detector remains an interesting question that requires further studies.

Bibliography

[1] G. E. Moore, "Cramming more components onto integrated circuits," *Electronics*, vol. 38, no. 8, p. 114, 1965.

[2] S. E. Thompson and S. Parthasarathy, "Moore's law: the future of Si microelectronics," *Materials Today*, vol. 9, no. 6, pp. 20 – 25, 2006.

[3] M. Kastner, "The single electron transistor and artificial atoms," *Annalen der Physik*, vol. 9, no. 11-12, pp. 885–894, 2000.

[4] J. Clarke and F. K. Wilhelm, "Superconducting quantum bits," *Nature*, vol. 453, pp. 1031–1042, 06 2008.

[5] P. Y. Yu and M. Cardona, *Fundamentals of Semiconductors*. Springer, 2010.

[6] M. Tinkham, *Introduction to Superconductivity: Second Edition*. Dover Books on Physics, Dover Publications, 2004.

[7] J. P. Pekola, "Towards quantum thermodynamics in electronic circuits," *Nature Physics*, vol. 11, pp. 118–123, 02 2015.

[8] K. L. Viisanen, S. Suomela, S. Gasparinetti, O.-P. Saira, J. Ankerhold, and J. P. Pekola, "Incomplete measurement of work in a dissipative two level system," *New Journal of Physics*, vol. 17, no. 5, p. 055014, 2015.

[9] P. Yang, R. Yan, and M. Fardy, "Semiconductor nanowire: What's next?," *Nano Letters*, vol. 10, no. 5, pp. 1529–1536, 2010.

[10] T. Bryllert, L. Samuelson, L. E. Jensen, and L. Wernersson, "Vertical high mobility wrap-gated InAs nanowire transistor," in *63rd Device Research Conference Digest, 2005. DRC '05.*, vol. 1, pp. 157–158, June 2005.

[11] C. Thelander, L. E. FrÖbergFroberg, C. Rehnstedt, L. Samuelson, and L. E. Wernersson, "Vertical enhancement-mode InAs nanowire field-effect transistor

with 50-nm wrap gate," *IEEE Electron Device Letters*, vol. 29, pp. 206–208, March 2008.

[12] R. Yan, D. Gargas, and P. Yang, "Nanowire photonics," *Nat Photon*, vol. 3, pp. 569–576, 10 2009.

[13] N. P. Dasgupta, J. Sun, C. Liu, S. Brittman, S. C. Andrews, J. Lim, H. Gao, R. Yan, and P. Yang, "25th anniversary article: Semiconductor nanowires – synthesis, characterization, and applications," *Advanced Materials*, vol. 26, no. 14, pp. 2137–2184, 2014.

[14] V. Mourik, K. Zuo, S. M. Frolov, S. R. Plissard, E. P. A. M. Bakkers, and L. P. Kouwenhoven, "Signatures of Majorana fermions in hybrid superconductor-semiconductor nanowire devices," *Science*, vol. 336, no. 6084, pp. 1003–1007, 2012.

[15] F. Hassler, A. R. Akhmerov, and C. W. J. Beenakker, "The top-transmon: a hybrid superconducting qubit for parity-protected quantum computation," *New Journal of Physics*, vol. 13, no. 9, p. 095004, 2011.

[16] O.-P. Saira, *Electrostatic control of quasiparticle transport in superconducting hybrid nanostructures*. PhD thesis, Aalto University, 2013.

[17] B. Josephson, "Possible new effects in superconductive tunnelling," *Physics Letters*, vol. 1, no. 7, pp. 251 – 253, 1962.

[18] H. Meissner", "Superconductivity of contacts with interposed barriers," *Physical Review*, vol. 117, no. 3, pp. 672–680, 1960.

[19] A. Andreev, "Thermal conductivity of the intermediate state of superconductors," *Zh. Eksp. Teor. Fiz.*, vol. 46, pp. 1823–1828, 1964.

[20] J. Peltonen, *Fluctuations, relaxation and proximity effect in superconducting circuits*. PhD thesis, Aalto University, 2011.

[21] F. Giazotto, T. T. Heikkilä, A. Luukanen, A. M. Savin, and J. P. Pekola, "Opportunities for mesoscopics in thermometry and refrigeration: Physics and applications," *Rev. Mod. Phys.*, vol. 78, pp. 217–274, Mar 2006.

[22] M. Meschke, J. T. Peltonen, H. Courtois, and J. P. Pekola, "Calorimetric readout of a superconducting proximity-effect thermometer," *Journal of Low Temperature Physics*, vol. 154, no. 5, pp. 190–198, 2009.

[23] M. D. Eisaman, J. Fan, A. Migdall, and S. V. Polyakov, "Invited review article: Single-photon sources and detectors," *Review of Scientific Instruments*, vol. 82, no. 7, p. 071101, 2011.

[24] J. Govenius, R. E. Lake, K. Y. Tan, and M. Möttönen, "Detection of zeptojoule microwave pulses using electrothermal feedback in proximity-induced Josephson junctions," *Phys. Rev. Lett.*, vol. 117, p. 030802, Jul 2016.

[25] S. Gasparinetti, K. L. Viisanen, O.-P. Saira, T. Faivre, M. Arzeo, M. Meschke, and J. P. Pekola, "Fast electron thermometry for ultrasensitive calorimetric detection," *Physical Review Applied*, vol. 3, no. 1, 2015.

[26] F. C. Wellstood, C. Urbina, and J. Clarke, "Hot-electron effects in metals," *Phys. Rev. B*, vol. 49, no. 9, pp. 5942–5955, 1994.

[27] K. L. Viisanen, "Fast electron thermometry towards single shot calorimetric detection of energy in the microwave regime." Midterm Review.

[28] Y. Xia, P. Yang, Y. Sun, Y. Wu, B. Mayers, B. Gates, Y. Yin, F. Kim, and H. Yan, "One-dimensional nanostructures: Synthesis, characterization, and applications," *Advanced Materials*, vol. 15, no. 5, pp. 353–389, 2003.

[29] L. O. Olsson, C. B. M. Andersson, M. C. Håkansson, J. Kanski, L. Ilver, and U. O. Karlsson, "Charge accumulation at InAs surfaces," *Phys. Rev. Lett.*, vol. 76, pp. 3626–3629, May 1996.

[30] C. A. Mead and W. G. Spitzer, "Fermi level position at semiconductor surfaces," *Phys. Rev. Lett.*, vol. 10, pp. 471–472, Jun 1963.

[31] S. Roddaro, A. Pescaglini, D. Ercolani, L. Sorba, F. Giazotto, and F. Beltram, "Hot-electron effects in InAs nanowire josephson junctions," *Nano Research*, vol. 4, no. 3, pp. 259–265, 2011.

[32] H. Y. Günel, I. E. Batov, H. Hardtdegen, K. Sladek, A. Winden, K. Weis, G. Panaitov, D. Grützmacher, and T. Schäpers, "Supercurrent in Nb/InAs-nanowire/Nb Josephson junctions," *Journal of Applied Physics*, vol. 112, no. 3, 2012.

[33] Y.-J. Doh, J. A. van Dam, A. L. Roest, E. P. A. M. Bakkers, L. P. Kouwenhoven, and S. De Franceschi, "Tunable supercurrent through semiconductor nanowires," *Science*, vol. 309, no. 5732, pp. 272–275, 2005.

[34] R. S. Wagner and W. C. Ellis, "Vapor-liquid-solid mechanism of single crystal growth," *Applied Physics Letters*, vol. 4, no. 5, 1964.

[35] M. Yazawa, M. Koguchi, A. Muto, and K. Hiruma, "Semiconductor nanowhiskers," *Advanced Materials*, vol. 5, no. 7-8, pp. 577–580, 1993.

[36] P. Krogstrup, N. L. B. Ziino, W. Chang, S. M. Albrecht, M. H. Madsen, E. Johnson, J. Nygård, C. M. Marcus, and T. S. Jespersen, "Epitaxy of semiconductor–superconductor nanowires," *Nat Mater*, vol. 14, pp. 400–406, 04 2015.

[37] T. D. Stanescu, R. M. Lutchyn, and S. Das Sarma, "Soft superconducting gap in semiconductor-based majorana nanowires," *Phys. Rev. B*, vol. 90, p. 085302, Aug 2014.

[38] F. Pobell, *Matter and Methods at Low Temperatures*. Springer, 2007.

[39] P. Das, R. B. de Ouboter, and K. W. Taconis, *A Realization of a London-Clarke-Mendoza Type Refrigerator*, pp. 1253–1255. Boston, MA: Springer US, 1965.

[40] W. Chang, *Superconducting proximity effect in InAs nanowires*. PhD thesis, Harvard University, 2014.

[41] T. W. Larsen, K. D. Petersson, F. Kuemmeth, T. S. Jespersen, P. Krogstrup, J. Nygård, and C. M. Marcus, "Semiconductor-nanowire-based superconducting qubit," *Phys. Rev. Lett.*, vol. 115, p. 127001, Sep 2015.

[42] J. Pekola and J. Kauppinen, "Insertable dilution refrigerator for characterization of mesoscopic samples," *Cryogenics*, vol. 34, pp. 843–845, 10 1994.

[43] H. Courtois, M. Meschke, J. T. Peltonen, and J. P. Pekola, "Origin of hysteresis in a proximity Josephson junction," *Phys. Rev. Lett.*, vol. 101, p. 067002, Aug 2008.